arXiv:1412.2786v1 [q-bio.BM] 8 Dec 2014

Fast and Anisotropic Flexibility-Rigidity Index for Protein Flexibility and Fluctuation Analysis

Kristopher Opron[1], Kelin Xia[2] and Guo-Wei Wei[1,2,3] *
[1] Department of Biochemistry and Molecular Biology
Michigan State University, MI 48824, USA
[2] Department of Mathematics
Michigan State University, MI 48824, USA
[3] Department of Electrical and Computer Engineering
Michigan State University, MI 48824, USA

December 10, 2014

Abstract

Protein structural fluctuation, typically measured by Debye-Waller factors, or B-factors, is a manifestation of protein flexibility, which strongly correlates to protein function. The flexibility-rigidity index (FRI) is a newly proposed method for the construction of atomic rigidity functions required in the theory of continuum elasticity with atomic rigidity (CEWAR), which is a new multiscale formalism for describing excessively large biomolecular systems. The FRI method analyzes protein rigidity and flexibility and is capable of predicting protein B-factors without resorting to matrix diagonalization. A fundamental assumption used in the FRI is that protein structures are uniquely determined by various internal and external interactions, while the protein functions, such as stability and flexibility, are solely determined by the structure. As such, one can predict protein flexibility without resorting to the protein interaction Hamiltonian. Consequently, bypassing the matrix diagonalization, the original FRI has a computational complexity of $\mathcal{O}(N^2)$. This work introduces a fast FRI (fFRI) algorithm for the flexibility analysis of large macromolecules. The proposed fFRI further reduces the computational complexity to $\mathcal{O}(N)$. Additionally, we propose anisotropic FRI (aFRI) algorithms for the analysis of protein collective dynamics. The aFRI algorithms admit adaptive Hessian matrices, from a completely global $3N \times 3N$ matrix to completely local 3×3 matrices. However, these local 3×3 matrices have built in much non-local correlation. Eigenvectors obtained the proposed aFRI lagorithms are able to demonstrate collective motions. Moreover, we investigate the performance of FRI by employing four families of radial basis correlation functions. Both parameter optimized and parameter-free FRI methods are explored. Furthermore, we compare the accuracy and efficiency of FRI with some established approaches to flexibility analysis, namely, normal mode analysis (NMA) and Gaussian network model (GNM). The accuracy of the FRI method is tested using four sets of proteins, three sets of relatively small-, medium- and large-sized structures and an extended set of 365 proteins. A fifth set of proteins is used to compare the efficiency of the FRI, fFRI, aFRI and GNM methods. Intensive validation and comparison indicate that the FRI, particularly the fFRI, is orders of magnitude more efficient and about 10% more accurate overall than some of the most popular methods in the field. The proposed fFRI is able to predict B-factors for α-carbons of the HIV virus capsid (313,236 residues) in less than 30 seconds on a single processor using only one core. Finally, we demonstrate the application of FRI and aFRI to protein domain analysis.

Key words: Protein flexibility, Thermal fluctuation, Continuum elasticity, Atomic rigidity, Multiscale.

*Address correspondences to Guo-Wei Wei. E-mail:wei@math.msu.edu

I Introduction

Proteins provide the structural basis for living organisms and are essential research subjects of the biological sciences. Although the original sequence-structure-function dogma[2] has been seriously challenged,[8,32] the protein structure, in either folded or unfolded form, still determines its function. Therefore, the understanding of the structure of a protein holds the key to the prediction of the protein's function.[27,45] Unfortunately, it remains a major challenge in the biological sciences to predict a protein's functions from its known structure.

There are a few essential factors, including protein geometry, electrostatics, and flexibility, that strongly correlate to protein function. There is no need to elaborate on the importance of protein geometry and electrostatics to protein function and dynamics. However, the impact of protein flexibility to protein function is often underestimated or even overlooked. In general, protein flexibility is the ability to deform from the equilibrium state under external forces, such as docking of ligands, docking with other proteins or random bombardments of small molecules in liquid and/or gas phases and lattice phonons in a solid phase.[13] Under physiological conditions, proteins experience everlasting motion or structural fluctuation in a wide variety of spatiotemporal scales because of their flexibility and uninterrupted external forces. However, at absolute zero temperature, there is no protein motion or fluctuation. Therefore protein motion or fluctuation is just the molecule's response to the external stimuli, while protein flexibility is an intrinsic property of the structure. In fact, protein flexibility varies from protein to protein and is a signature of the protein. In a given protein, flexibility can be different from atom to atom, from residue to residue and from domain to domain. Typically, the performance of a theoretical model for protein flexibility analysis can be validated via its prediction of protein structural fluctuation.

X-ray crystallography is one of the most important techniques for protein flexibility analysis. The atomic mean-square-fluctuations are reflected in X-ray diffraction or other diffraction data and can be estimated in terms of the Debye-Waller factor, also known as the B-factor or temperature factor. Typically, reported B-factors are not corrected for the variations in atomic diffraction cross sections and chemical stability during the diffraction data collection, which perhaps contributes to the fact that all-atom models usually do not work as well as coarse-grained models in the B-factor prediction.[28] Nuclear magnetic resonance (NMR) is another important method, which is particularly valuable for flexibility analysis under physiological conditions. NMR is able to investigate protein flexibility at a variety of timescales.

Apart from experimental approaches, a number of theoretical methods have been developed for flexibility analysis and B-factor prediction in the past. Protein collective motion and fluctuation can be elucidated by molecular dynamics (MD), which has considerably expanded our understanding of the conformational landscapes of proteins. However, the excessively large number of degrees of freedom associated with the all-atom representation and long time integration becomes computationally inefficient with increasing size of the system and can obscure larger scale motions. Alternative time-independent approaches, such as normal mode analysis (NMA),[7,15,23,39] graph theory[19] and elastic network model (ENM)[41] theories, including Gaussian network model (GNM)[4,5,12] and anisotropic network model (ANM)[3], have been developed for protein flexibility analysis in the past few decades. These methods can be derived from their corresponding Newton's equations by using the time-harmonic approximation.[28] The low order eigenmodes computed from diagonalizing the Kirchhoff matrix or the Hessian matrix can shed light on the long-time behavior of the protein dynamics beyond the reach of MD simulations.[5,7,23,39,41] Coarse-grained based ENM and GNM approaches have become popular recently due to their simplified potential and computational efficiency.[3–5,16,24,37] It was shown that the GNM is about one order more efficient than most other approaches.[48] Improvements to these approaches have been developed for many aspects, including crystal periodicity and cofactor corrections,[17,21,22,35] and density - cluster rotational - translational blocking.[11] These approaches have been applied to the study of large proteins or protein complexes, such as, hemoglobin,[47] F1 ATPase,[10,50] chaperonin GroEL,[20,49] viral capsids,[29,36] and ribosome.[38,43] Flexibility also plays an important role in stability[25] and docking analysis.[14] For further detail in their status and application, the reader is referred to recent review papers.[9,26,34,48]

Recently, we have developed a new multiscale formalism called continuum elasticity with atomic rigidity (CEWAR) for the elastic analysis of excessively large macromolecules. In the CEWAR approach, a continuous atomic rigidity function is required to characterize the shear modulus in the stress tensor of elasticity equations. To this end, a simple method, called flexibility-rigidity index (FRI), is introduced to evaluate macromolecular flexibility and rigidity.[46] We noted after the publication of our earlier work[46] that the name of "flexibility index" was proposed independently by von der Lieth et al.[42] and Jacobs et al.[19] for two different quantities to describe bond strengths. Both of these flexibility indices are distinct from our proposed FRI. The FRI is a solely structural based algorithm that does not reconstruct any protein interaction Hamiltonian. Only elementary arithmetics is

needed in the FRI method for proteins. In particular, the FRI prediction of protein B-factors does not require a stringently minimized structure and time consuming matrix diagonalization or matrix decomposition, nor does it involve any training procedure. Two types of monotonically decaying correlation functions, namely, exponential type and Lorentz type, have been utilized previously for the construction of protein correlation matrix. Parameter ranges for the FRI have been extensively tested and the performance of the FRI for protein B-factor prediction has been carefully validated with a set of 263 proteins.[46] It is found that for residue based B-factor prediction, the FRI can be made parameter free. However, it is not clear how the FRI compares to alternative approaches in the field, particularly the state of the art methods such as GNM and NMA.

One of the objectives of the present work is to introduce a fast FRI (fFRI) algorithm by using appropriate data structures. Computational efficiency is a central issue. The computational complexity of the proposed fFRI is of $\mathcal{O}(N)$, compared to that of $\mathcal{O}(N^2)$ for the original FRI algorithm and of $\mathcal{O}(N^3)$ for the GNM, where N is the number of atoms. We use a cell lists approach[1] to reduce the computational complexity. Another objective is to introduce anisotropic FRI (aFRI) algorithms for the motion analysis of biomolecules. Unlike ANM,[3,28] which is completely global and has $3N \times 3N$ elements in its Hessian matrix, the proposed aFRI algorithms have adaptive Hessian matrices, which vary from completely global to completely local. Despite of the localization, there are collective motions in three sets of eigenvectors. The other objective of the present work is to further analyze the performance of the FRI methods for protein B-factor prediction. To this end, we examine the accuracy of FRI algorithms associated with four families of correlation functions and carry out a comparative study of the FRI and fFRI vs. other cutting edge approaches, namely, NMA and GNM. Our investigation concerns three issues, i.e., accuracy, reliability, and efficiency in the protein B-factor prediction. Finally, we also demonstrate the applications of the FRI and aFRI to protein domain analysis.

The rest of this paper is organized as follows. Section II is devoted to methods and algorithms. To establish notation and facilitate further discussion, the FRI approach is briefly discussed. We present a new simplified version of the FRI that is relevant to the B-factor prediction and visualization analysis studied in this work. Anisotropic FRI algorithms are proposed via two different ways. The fFRI algorithm is developed by using appropriate data structures to avoid the evaluation of insignificant correlation matrix elements, which leads to a sparse fFRI matrix. In Section III, we first analyze the behavior of a few FRI correlation functions. Additionally, we examine the parameter dependence of some FRI correlation functions. Moreover, the performance of fFRI is investigated. Further, we provide a comprehensive comparison of our FRI and other established methods. We adopted three protein sets corresponding to relatively small-, medium-, and large-sized structures, proposed in the literature.[28] We also utilize an extended set of 365 proteins to further evaluate the performance of various methods. Furthermore, the computational complexities of FRI, fFRI and GNM are compared over a set of 44 proteins. Finally, we show that the FRI offers a distinguished visualization of biomolecular structure and interaction. In Section IV, we demonstrate the usefulness of the FRI and aFRI by carrying out an in-depth study of protein domains. This paper ends with concluding remarks.

II Theory and algorithm

In the continuum elasticity with atomic rigidity (CEWAR) model, the dynamics of a biomolecular system under the given force $\mathbf{f}$ is governed by the equation of motion[46]

$$\rho\ddot{\mathbf{w}} = \left[\nabla\lambda\nabla\cdot\mathbf{w} + \nabla\mu\cdot[\nabla\mathbf{w} + (\nabla\mathbf{w})^T] + (\lambda+\mu)\nabla\nabla\cdot\mathbf{w} + \mu\nabla^2\mathbf{w}\right] + \mathbf{f}, \tag{1}$$

where ρ is the density of the macromolecule, $\mathbf{w}$ is the displacement, and $\lambda = \lambda(\mathbf{r})$ and $\mu = \mu(\mathbf{r})$ are respectively bulk modulus and shear modulus. The FRI algorithm was proposed to evaluate the shear modulus, i.e., rigidity.

This section describes the theory and algorithm underpinning the FRI method. We first briefly review the FRI theory to establish notation. Then, two anisotropic FRI algorithms are introduced for the analysis of the anisotropic motions of biomolecules. Finally, A fast FRI algorithm is proposed to reduce the computational complexity of the original FRI.

II.A Flexibility-rigidity index

We consider proteins as examples to illustrate our FRI algorithm, although other biomolecules, such as DNA and RNA, can be similarly treated with a minor modification of our algorithm. We are particularly interested in a coarse-grained representation. However, methods for a full atom description can be formulated as well.

We seek a structure based algorithm to convert protein geometry into protein topology. To this end, we consider a protein with N C_α atoms. Their locations are represented by $\{\mathbf{r}_j | \mathbf{r}_j \in \mathbb{R}^3, j = 1, 2, \cdots, N\}$. We denote $\|\mathbf{r}_i - \mathbf{r}_j\|$ the Euclidean space distance between ith C_α atom and the jth C_α atom. The distance geometry of

protein C_α atoms is utilized to establish the topology connectivity by using monotonically decreasing radial basis functions,

$$C_{ij} = \Phi(\|\mathbf{r}_i - \mathbf{r}_j\|; \eta_{ij}), \tag{2}$$

where η_{ij} is a characteristic distance between particles, and $\Phi(\|\mathbf{r}_i - \mathbf{r}_j\|; \eta_{ij})$ is a correlation function, which is, in general, a real-valued monotonically decreasing function. As a correlation function, it satisfies

$$\Phi(\|\mathbf{r}_i - \mathbf{r}_i\|; \eta_{ii}) = 1 \tag{3}$$

$$\Phi(\|\mathbf{r}_i - \mathbf{r}_j\|; \eta_{ij}) = 0 \quad \text{as} \quad \|\mathbf{r}_i - \mathbf{r}_j\| \to \infty. \tag{4}$$

Delta sequences of the positive type discussed in an earlier work[44] are all good choices. For example, one can use generalized exponential functions

$$\Phi(\|\mathbf{r}_i - \mathbf{r}_j\|; \eta_{ij}) = e^{-(\|\mathbf{r}_i - \mathbf{r}_j\|/\eta_{ij})^\kappa}, \quad \kappa > 0 \tag{5}$$

and generalized Lorentz functions

$$\Phi(\|\mathbf{r}_i - \mathbf{r}_j\|; \eta_{ij}) = \frac{1}{1 + (\|\mathbf{r}_i - \mathbf{r}_j\|/\eta_{ij})^\upsilon}, \quad \upsilon > 0. \tag{6}$$

Essentially, the correlation between any two particles should decay according to their distance. Therefore, many other alternatives can be used and some of them are investigated in Section III.

The correlation map or cross correlation is an important quantity for the GNM. We can define a similar correlation map by setting $\mathbf{C} = \{C_{ij}\}, i, j = 1, 2, \cdots, N$. The correlation map measures the connectivity of C_αs in the protein. The similarity and difference of the present correlation map and that of the GNM are studied in Section III.

We define an atomic rigidity index μ_i as the summation of topological connectivity

$$\mu_i = \sum_{j=1}^{N} w_{ij} \Phi(\|\mathbf{r}_i - \mathbf{r}_j\|; \eta_{ij}), \quad \forall i = 1, 2, \cdots, N, \tag{7}$$

where w_{ij} is a weight function related to the atomic type, The atomic rigidity index μ_i manifests the rigidity or stiffness at the ith atom. In a general sense, the atomic rigidity index reflects the total interaction strength, including both bonded and non-bonded contributions. It is quite straightforward to define the averaged molecular rigidity index as a summation of atomic rigidity indices

$$\bar{\mu}_{\text{MRI}} = \frac{1}{N} \sum_{i=1}^{N} \mu_i. \tag{8}$$

The averaged molecular rigidity index can be used to predict molecular thermal stability, bulk modulus, density (compactness), boiling points of isomers, the ratio of surface area over volume, surface tension, etc. A detailed investigation of these aspects is beyond the scope of the present work.

We are now ready to define a position dependent shear modulus

$$\mu(\mathbf{r}) = \sum_{j=1}^{N} w_j(\mathbf{r}) \Phi(\|\mathbf{r} - \mathbf{r}_j\|; \eta_{ij}), \quad \mathbf{r} \in \Omega_E, \tag{9}$$

where $w_j(\mathbf{r})$ is a weight function, $\mathbf{r}$ is in the proximity of $\mathbf{r}_i$ and Ω_E is the macromolecular domain. In order to determine $w_j(\mathbf{r})$, we define an average rigidity (or averaged rigidity index function) by

$$\bar{\mu} = \frac{1}{V} \int \mu(\mathbf{r}) d\mathbf{r}, \tag{10}$$

where V is the volume of the macromolecule. If $w_j(\mathbf{r})$ is a constant, its value can be uniquely determined by a comparison of $\bar{\mu}$ with experimental shear modulus[33] for a given macromolecule and correlation function.

We also define an atomic flexibility index as

$$f_i = \frac{1}{\mu_i}, \quad \forall i = 1, 2, \cdots, N. \tag{11}$$

Since the flexibility at each atom is proportional to its temperature fluctuation, we can express B-factors as

$$B_i^t = a f_i + b, \quad \forall i = 1, 2, \cdots, N \tag{12}$$

where $\{B_i^t\}$ are theoretically predicted B-factors, and a and b are two constants to be determined by a simple linear regression.

We can also define the averaged molecular flexibility index (MFI) as a summation of atomic flexibility indices

$$\bar{f}_{\mathrm{MFI}} = \frac{1}{N} \sum_{i=1}^{N} f_i. \tag{13}$$

MFI should correlate with molecular stability and energy.

For the purpose of visualization, we define a continuous atomic flexibility function as

$$F(\mathbf{r}) \quad = \quad \sum_{j=1}^{N} B_i^t \Psi(\|\mathbf{r} - \mathbf{r}_j\|), \quad \mathbf{r} \in \Omega_E. \tag{14}$$

where $\Psi(\|\mathbf{r} - \mathbf{r}_j\|)$ is a general interpolation function for scattered data. Wavelets, spline functions, and modified Shepard's method[30,40] can be employed for the interpolation. One can map $f(\mathbf{r})$ to the molecular surface to visualize the protein flexibility.[46] Alternatively, one can compute the continuous atomic flexibility function by

$$F(\mathbf{r}) \quad = \quad \frac{1}{\sum_{j=1}^{N} w_j(\mathbf{r}) \Phi(\|\mathbf{r} - \mathbf{r}_j\|; \eta_{ij})}, \quad \mathbf{r} \in \Omega_E. \tag{15}$$

II.B Anisotropic flexibility-rigidity index

In this section, we propose a new anisotropic model based on our FRI theory. In existing anisotropic methods, the Hessian matrix is always global, i.e., the matrix contains all the $3N \times 3N$ elements for N particles in molecule. In our aFRI model, the Hessian matrix is inherently local and adaptive. Its size may vary from 3×3 for a completely local aFRI to $3N \times 3N$ for a complete global aFRI, depending on the need of a physical problem.

Let us partition all the N particles in a molecule into a total of M clusters $\{c_1, c_2, \cdots, c_k, \cdots, c_M\}$. Cluster c_k has N_k particles or atoms so that $N = \sum_{k=1}^{M} N_k$. A cluster may be of physical interest, i.e., an alpha helix, a domain, or a binding site of a protein. One of two extreme cases is that there is only one particle in each cluster. We therefore have N cluster. The other case is that there is only one cluster, i.e., the whole molecule. The essential idea is to develop a Hessian matrix for each cluster individually without the information about other cluster properties (However, information for nearby particles outside the cluster is still required). For example, if we are interested in the thermal fluctuation of a particular cluster c_k with N_k particles or atoms, we can find $3N_k$ eigenvectors for the cluster. Let us keep in mind that each position vector in $\mathbb{R}^3$ has three components, i.e., $\mathbf{r} = (x, y, z)$. We denote

$$\Phi_{uv}^{ij} = \frac{\partial}{\partial u_i} \frac{\partial}{\partial v_j} \Phi(\|\mathbf{r}_i - \mathbf{r}_j\|; \eta_{ij}), \quad u, v = x, y, z; i, j = 1, 2, \cdots, N. \tag{16}$$

Note that for each given ij, we define $\Phi^{ij} = \left(\Phi_{uv}^{ij}\right)$ as a local anisotropic matrix

$$\Phi^{ij} = \begin{pmatrix} \Phi_{xx}^{ij} & \Phi_{xy}^{ij} & \Phi_{xz}^{ij} \\ \Phi_{yx}^{ij} & \Phi_{yy}^{ij} & \Phi_{yz}^{ij} \\ \Phi_{zx}^{ij} & \Phi_{zy}^{ij} & \Phi_{zz}^{ij} \end{pmatrix}. \tag{17}$$

Since rigidity and flexibility can be both anisotropic, it is nature to propose two different aFRI algorithms based on rigidity Hessian matrix and flexibility Hessian matrix, respectively.

II.B.1 Anisotropic rigidity

The anisotropic rigidity is defined by a rigidity Hessian matrix for an arbitrary cluster c_k. Let us denote $\left(\mu_{uv}^{ij}(c_k)\right)$ a rigidity Hessian matrix for cluster c_k. Its elements are chosen as

$$\mu_{uv}^{ij}(c_k) = -w_{ij}\Phi_{uv}^{ij}, \qquad i,j \in c_k; i \neq j; u,v = x,y,z \tag{18}$$

$$\mu_{uv}^{ii}(c_k) = \sum_{j=1}^{N} w_{ij}\Phi_{uv}^{ij}, \qquad i \in c_k; u,v = x,y,z \tag{19}$$

$$\mu_{uv}^{ij}(c_k) = 0, \qquad i,j \notin c_k; u,v = x,y,z. \tag{20}$$

Hessian matrix $\left(\mu_{uv}^{ij}(c_k)\right)$ is of $3N_k \times 3N_k$ dimensions. Note that the diagonal part, $\mu_{uv}^{ii}(c_k)$, has built in information from all the particles in the system, even if the cluster is completely localized, i.e., $N_k = 1,\ \forall k$.

An immediate test of the anisotropic rigidity is to check if it works for the B-factor prediction. To this end, we collect the diagonal terms of the rigidity Hessian matrix

$$\mu_{\rm diag}^{i} = \mathrm{Tr}\left(\mu_{uv}^{i}\right) \tag{21}$$

$$= \sum_{j=1}^{N} w_{ij}\left[\Phi_{xx}^{ij} + \Phi_{yy}^{ij} + \Phi_{zz}^{ij}\right]. \tag{22}$$

We then define a set of anisotropic rigidity (AR) based flexibility indices by

$$f_i^{\rm AR} = \frac{1}{\mu_{\rm diag}^{i}}. \tag{23}$$

B-factors can be predicted with a set of $\{f_i^{\rm AR}\}$ by using the linear regression in Eq. (12).

II.B.2 Anisotropic flexibility

To analyze biomolecular anisotropic motions in parallel to ANM, we need to examine their anisotropic flexibility. To this end, we further define a flexibility Hessian matrix $\mathbf{F}(c_k)$ for cluster c_k as

$$\mathbf{F}^{ij}(c_k) = -\tfrac{1}{w_{ij}}(\Phi^{ij})^{-1}, \qquad i,j \in c_k; i \neq j; u,v = x,y,z \tag{24}$$

$$\mathbf{F}^{ii}(c_k) = \sum_{j=1}^{N} \tfrac{1}{w_{ij}}(\Phi^{ij})^{-1}, \qquad i \in c_k; u,v = x,y,z \tag{25}$$

$$\mathbf{F}^{ij}(c_k) = 0, \qquad i,j \notin c_k; u,v = x,y,z. \tag{26}$$

where $(\Phi^{ij})^{-1}$ denote the unscaled inverse of matrix Φ^{ij} such that $\Phi^{ij}(\Phi^{ij})^{-1} = |\Phi^{ij}|$. Similar to the anisotropic rigidity, the diagonal part $\mathbf{F}^{ii}(c_k)$ has built in information from all particles in the system. Therefore, even if the partition of clusters is completely localized (i.e., N clusters), certain correlation among atomic motions is retained. By diagonalizing $\mathbf{F}(c_k)$, we obtain $3N_k$ eigenvectors for the N_k particles in cluster c_k. Since the selection of c_k is arbitrary, eigenvectors of all other clusters can be attained using the same procedure.

To obtain the B-factor prediction from this anisotropic flexibility, we define a set of anisotropic flexibility (AF) based flexibility indices by

$$f_i^{\rm AF} = \mathrm{Tr}\left(\mathbf{F}(c_k)\right)^{ii}, \tag{27}$$

$$= \left(\mathbf{F}(c_k)\right)_{xx}^{ii} + \left(\mathbf{F}(c_k)\right)_{yy}^{ii} + \left(\mathbf{F}(c_k)\right)_{zz}^{ii}. \tag{28}$$

Then Eq. (12) is employed to obtain B-factor predictions.

In this work, we only consider the coarse-grained model in which each residue is represented by its C_α. To further simply the model, the differences between residues are ignored. The parameter w_{ij} is assumed to be 1 and η_{ij} is set to a constant η.

II.C Fast FRI algorithm

As discussed in our earlier work,[46] the original FRI algorithm has the computational complexity of $\mathcal{O}(N^2)$, mainly due to the construction of the correlation matrix. In the present work, we propose a fast FRI (fFRI) algorithm, which computes only the significant elements of the correlation matrix and at the same time maintains the accuracy of our method. As a result, the computational complexity of our fFRI algorithm is of $\mathcal{O}(N)$.

The essential idea is to partition the residues in a protein into cubic boxes according to their spatial locations. For each residue in a given box, we only compute its correlation matrix elements with all residues within the given

box and with all residues in the adjacent 26 boxes. The accuracy and efficiency of this approach are determined by the box dimension. We select a box size of R such that

$$\Phi(R;\eta) \leq \varepsilon \tag{29}$$

where $\varepsilon > 0$ is a given truncation error. Therefore, for generalized exponential functions (5), we have

$$R \geq \eta \left(\ln \frac{1}{\varepsilon} \right)^{\frac{1}{\kappa}}. \tag{30}$$

If we set $\varepsilon = 10^{-2}$, we have $R \approx 4.6\eta$ for $\kappa = 1$ and $R \approx 2.15\eta$ for $\kappa = 2$. Note that different κ values have different optimal η values. The higher the κ value is, the larger the optimal η is.

Similarly, for generalized Lorentz functions (6), we choose the box size

$$R \geq \eta \left(\frac{1-\varepsilon}{\varepsilon} \right)^{\frac{1}{\upsilon}}. \tag{31}$$

Again, if we set $\varepsilon = 10^{-2}$, we have $R \approx 10\eta$ for $\upsilon = 2$ and $R \approx 4.6\eta$ for $\upsilon = 3$.

An optimal R should balance the accuracy and efficiency. In Section III.B, it is found that the selection of $R = 12$Å is near optimal for both exponential and Lorentz functions. In Algorithm 1, we present a pseudocode to illustrate the truncation algorithm of the fFRI.

III Numerical experiments

In this section, we validate the FRI approach for protein B-factor prediction by a comparison of its performance with that of two established methods, namely NMA and GNM. We consider the accuracy, reliability and efficiency of these methods. It is well known that the computational complexity of matrix diagonalization is asymptotically close to $\mathcal{O}(N^3)$, while that of correlation map construction and two-parameter linear regression given in Eq. (12) is asymptotically $\mathcal{O}(N^2)$. The computational complexity of the proposed fFRI algorithm is further reduced to $\mathcal{O}(N)$. Therefore, there is a dramatic reduction in the computational complexity. We demonstrate that the FRI method outperforms other methods in computational efficiency and is potentially useful for the flexibility analysis of excessively large macromolecules.

To test FRI against GNM and NMA, five sets of structures are utilized. Among them, three sets were used by Park, Jernigan and Wu in their comparative study.[28] These include relatively small-, medium- and large-sized sets of structures. A fourth set of 44 structures was created to test the efficiency of each algorithm. This set was created by randomly selecting protein-only structures from the Protein Data Bank database with varying size. The number of residues for proteins in this set range from 125 to 313,236 residues. The final set, called a superset, is a combination of sets including the three sets used by Park el al.,[28] the first 40 structures of the efficiency set and a set of 263 high-resolution structures used in earlier tests of the FRI method.[46] The total number of structures in the superset is 365 after the removal of duplicate structures.

To quantitatively assess the performance of the proposed FRI model for the B-factor prediction, we consider the correlation coefficient

$$C_c = \frac{\Sigma_{i=1}^{N} \left(B_i^e - \bar{B}^e\right)\left(B_i^t - \bar{B}^t\right)}{\left[\Sigma_{i=1}^{N}(B_i^e - \bar{B}^e)^2 \Sigma_{i=1}^{N}(B_i^t - \bar{B}^t)^2\right]^{1/2}}, \tag{32}$$

where $\{B_i^t, i = 1, 2, \cdots, N\}$ are a set of predicted B-factors by using the proposed method and $\{B_i^e, i = 1, 2, \cdots, N\}$ are a set of experimental B-factors read from the PDB file. Here $\bar{B}^t$ and $\bar{B}^e$ the statistical averages of theoretical and experimental B-factors, respectively.

III.A Analysis of FRI correlation functions

In order to further explore the FRI method, we test four types of correlation functions. Apart from the Lorentz and exponential functions, two alternative functions are employed in our study. All correlation functions equal to unit at the origin and are monotonically decreasing with respect to an increasing distance (r). Each correlation function is tested with a range of parameter values for each of 365 structures as listed in Table 1. The performance of the new correlation functions comes close to that of the exponential and Lorentz functions with the product of these two having the highest average correlation coefficient among alternative functions.

Algorithm 1 fFRI algorithm

Input: $atoms(N)$ ▷ XYZ coordinates from PDB file

$mincoor \leftarrow minval(atoms)$ ▷ Compute dimensions of bounding box
$maxcoor \leftarrow maxval(atoms)$
$R \leftarrow boxsize$ ▷ Set size of grid
$Nbox \leftarrow ceiling((maxcoor - mincoor)/R)$ ▷ Compute number of boxes in each direction

for $ii \leftarrow 1, Natoms$ **do**
  $i, j, k \leftarrow ceiling((atoms(ii) - mincoor/R))$ ▷ Count the number of atoms in each box
  $Natoms(i, j, k) \leftarrow Natoms(i, j, k) + 1$
end for

for $k \leftarrow 1, Nbox[3]$ **do**
  for $j \leftarrow 1, Nbox[2]$ **do**
    for $i \leftarrow 1, Nbox[1]$ **do**
      $allocate(box(i, j, k))$ ▷ Allocate space for each box
    end for
  end for
end for

for $ii \leftarrow 1, Natoms$ **do** ▷ Copy coordinates to appropriate box based on 3D coordinates
  $i, j, k \leftarrow ceiling((atoms(ii) - mincoor)/R)$
  $box(i, j, k) \leftarrow atoms(ii)$
end for

for $k \leftarrow 1, Nbox[3]$ **do** ▷ Iterate over boxes
  for $j \leftarrow 1, Nbox[2]$ **do**
    for $i \leftarrow 1, Nbox[1]$ **do**

      for $n_a \leftarrow 1, Natoms(i, j, k)$ **do** ▷ Iterate over atoms in current box

        for $n \leftarrow k - 1, k + 1$ **do** ▷ Iterate over adjacent boxes
          for $m \leftarrow j - 1, j + 1$ **do**
            for $l \leftarrow i - 1, i + 1$ **do**

              for $n_b \leftarrow 1, Natoms(l, m, n)$ **do** ▷ Iterate over atoms in adjacent boxes
                $dist \leftarrow distance(box(i, j, k)(n_a), box(l, m, n)(n_b))$
                $FRI(n_a) \leftarrow kernel(dist)$

              end for

            end for
          end for
        end for

      end for

    end for
  end for
end for

III.B Analysis of fFRI algorithms

To analyze the best parameter for Lorentz and exponential functions, we study their behavior in Fig. 1, where each function is tested over a range of parameters. For exponential type of functions, $\kappa = 1$ and $\eta = 3$Å give rise to a near optimal parameter-free FRI. Similarly, for Lorentz type of functions, $\upsilon = 3$, and $\eta = 3$Å offer near optimal results. It is seen from Fig. 1 that exponential functions are quite sensitive to η values, while Lorentz

Table 1: Comparison of average correlation coefficients computed from various correlation functions. Each function was tested across a range of parameters and the best score was saved for each structure and used to calculate the average over a set of 365 structures.

Correlation Function	Parameter Range	Average Correlation Coefficient
$e^{-(r/\eta)^\kappa}$	$1.0 \leq \eta \leq 10.0 \quad 0.5 \leq \kappa \leq 10.0$	0.676
$\frac{1}{1+(r/\eta)^\upsilon}$	$1.0 \leq \eta \leq 10.0 \quad 0.5 \leq \upsilon \leq 10.0$	0.673
$\frac{1}{1+(r/\eta)^\upsilon} e^{-(r/\eta)^\kappa}$	$1.0 \leq \eta, \upsilon, \kappa \leq 10.0$	0.670
$\frac{1}{\sqrt{1+(r/\eta)^\upsilon}}$	$1.0 \leq \eta, \upsilon \leq 10.0$	0.577

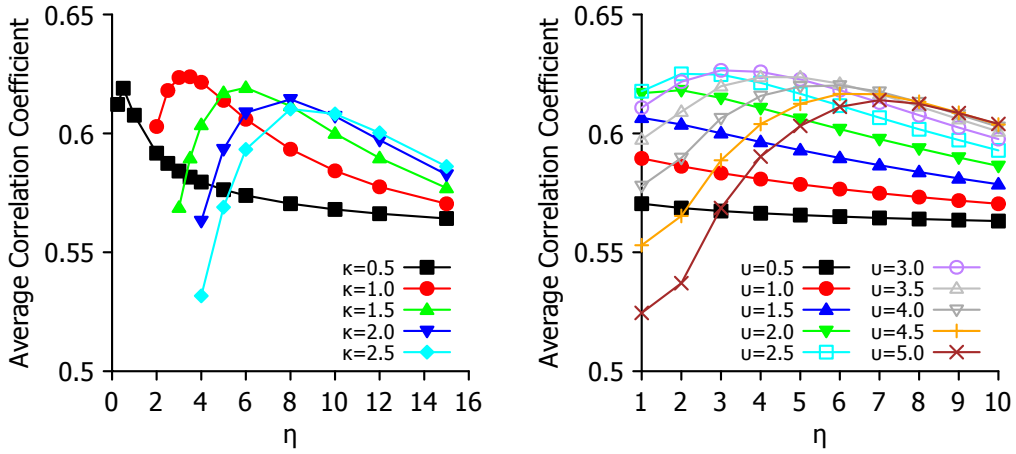

Figure 1: Parameter testing for exponential (Left chart) and Lorentz (Right chart) functions. Average correlation coefficient of B-factor predctions of 365 proteins is plot against choice of η for a range of values for κ or υ.

functions are relatively robust with respect to η. This study provides a basis for the selection of parameter free FRI (pfFRI) schemes.

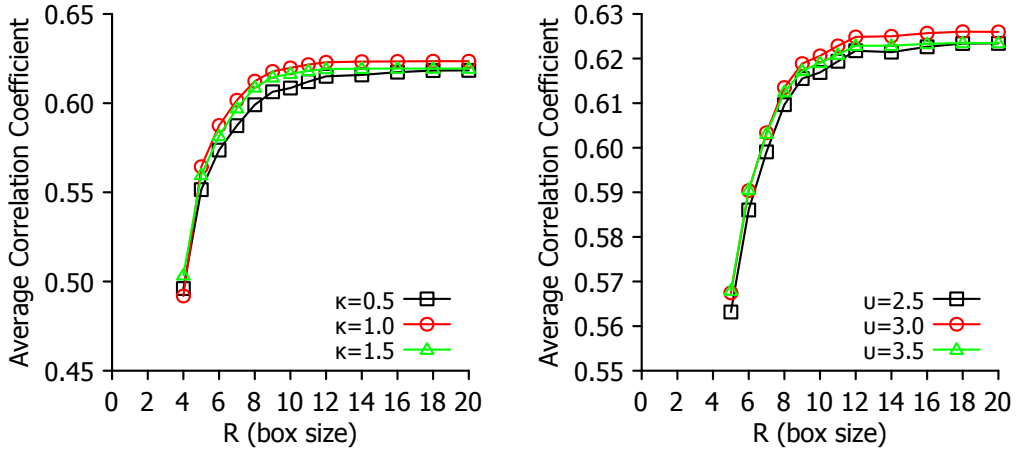

Figure 2: The impact of box size to the average correlation coefficient for a set of 365 proteins. The fFRI is examined over a range of values for parameters (κ and υ) to illustrate the relationship between accuracy and choice of box size R.

It is interesting to analyze the performance of the proposed fFRI in terms of accuracy and efficiency. To this end, we first explore the impact of box size to the correlation coefficients of a few fFRI schemes in Fig. 2. For each given κ and υ, the best η found in Fig. 1 is employed. It is seen from Fig. 2 that both exponential and Lorentz types of functions are able to achieve their near optimal performance at $R = 12$Å . Therefore, we recommend $R = 12$Å, $\eta = 3$Å and $\kappa = 1$ for the exponent type of fFRI method. Similarly, $R = 12$Å, $\eta = 3$Å and

$\upsilon = 3$ are near optimal for Lorentz type of fFRI methods.

III.C Comparison of B-factor predictions

III.C.1 FRI vs GNM and NMA

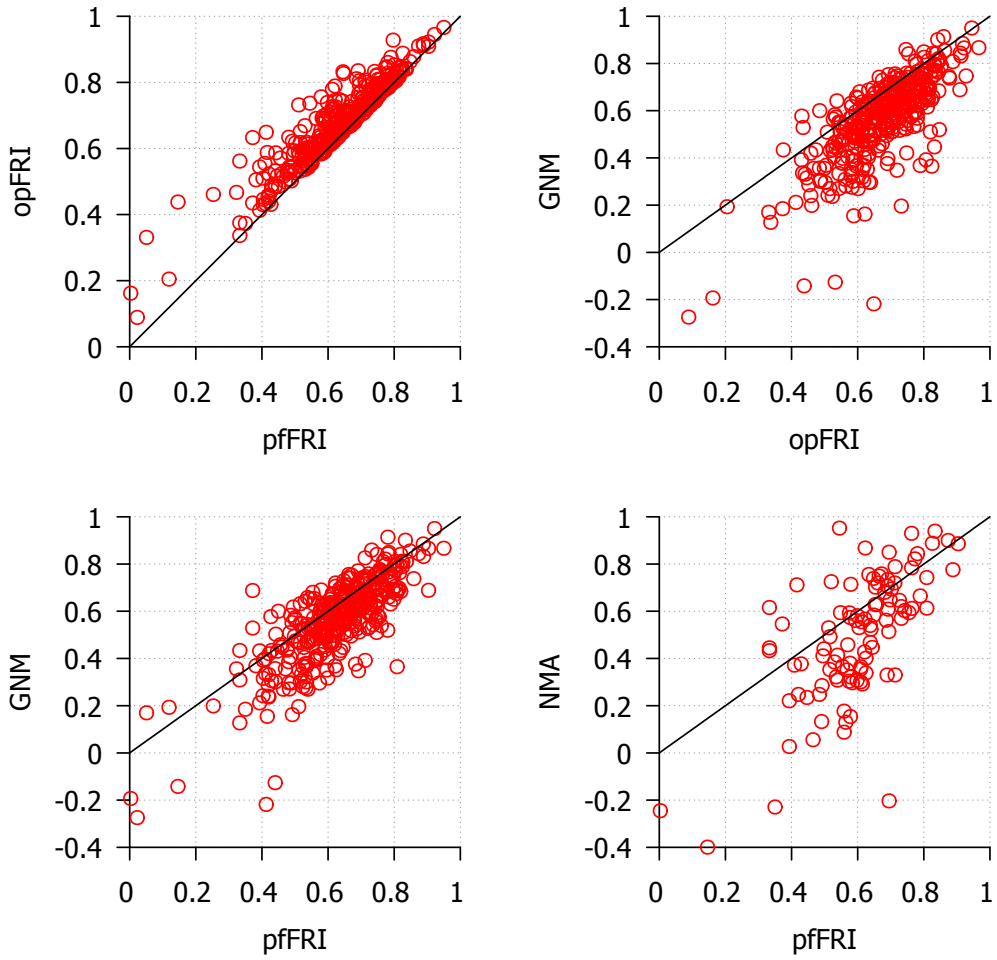

Figure 3: Comparison of correlation coefficients from B-factor prediction using GNM, coarse-grained (C_α) NMA and FRI methods. Top left: pfFRI vs opFRI for 365 proteins; Top right: opFRI vs GNM for 365 proteins; Bottom left: pfFRI vs GNM for 365 proteins; Bottom right: pfFRI vs NMA for three sets of proteins used by Park et al.[28] The correlation coefficients for NMA are adopted from Park et al.[28] for three sets of proteins. For optimal FRI, parameter υ is optimized for a range from 0.1 to 10.0. For the parameter free version of the FRI (pfFRI), we set $\upsilon = 3$ and $\eta = 3$Å. The line $y = x$ is included to aid in comparing scores.

In order to compare the FRI and GNM, we re-analyzed the structures from Park et al.[28] with the GNM method with a cutoff value of 7 Å, the same value used by the authors. It was found that some correlation coefficients were artificially low for GNM due to multiple coordinates for some C_α atoms in some PDB data and missing Cα atoms in others. To ensure a fair comparison between the FRI and GNM we re-analyzed the structures using GNM after processing the PDB files to fix these issues. We removed all but the highest occupancy coordinates for each atom and used every Cα atom from the original PDB files to run the GNM B-factor prediction code and calculate corrected correlation coefficients. In Tables 4, 5 and 6, optimal and parameter free FRI is compared to the GNM data reported by Park et al.[28] The newly calculated correlation coefficient is shown only if there is a significant improvement using our processed PDB files. On the other hand, Table 7 lists all correlation coefficients for GNM from our own tests using our processed PDB files. These correlation coefficients are typically the same as those reported by Park et al.[28] although some have changed. The use of our processed PDB files leads to a slight increase in the average scores for the GNM in our analysis.

To directly compare the FRI with GNM and NMA, we calculated the correlation coefficient of C_α B-factor

Table 2: Average correlation coefficients for C_α B-factor prediction with FRI, GNM and NMA for three structure sets from Park et al.[28] and a superset of 365 structures.

PDB set	opFRI	pfFRI	GNM	NMA
Small	0.667	0.594	0.541	0.480
Medium	0.664	0.605	0.550	0.482
Large	0.636	0.591	0.529	0.494
Superset	0.673	0.626	0.565	NA

predictions for the three structure sets taken from Park et al.[28] To further compare the FRI and GNM, we also calculated the accuracy of these two methods on a superset of 365 structures. Two versions of the FRI are used for these tests. The first, optimal FRI (opFRI), searches a wide range of parameters for the highest scoring parameter and the second, parameter free FRI (pfFRI), uses $\upsilon = 3$ and $\eta = 3$Å in all cases. The correlation coefficients for three sets proposed by Park et al. are reported in Tables 4, 5 and 6 for FRI, GNM and NMA. The results of the B-factor predictions for the superset are shown in Fig. 3. Using the top left chart as an example, both axises are correlation coefficients. For each circle, its x-coordinate is its correlation coefficient for pfFRI, while its y-coordinate is its correlation coefficient for opFRI. Since all circles are located above the diagonal line, opFRI always outperform pfFRI. The average correlation scores for optimal FRI, parameter free FRI, GNM and NMA for each set of structures are listed in Table 2. As shown in Table 2 and Fig. 3, opFRI outperforms pfFRI in many cases although the majority of structures have little difference in their score for each method. Both optimal and parameter free FRI methods outperform GNM and NMA for most structures. B-factor prediction with the FRI is most accurate for smaller structures (<70 residues). All three methods tend to perform worse as the structures get larger except in the case of NMA where the medium-sized structures scored slightly lower than the large-sized structures. This behavior is expected because as proteins get larger their structures become more complex and may include structural co-factors and more amino acid side chain interactions that contribute to the protein's stability. The coarse-grained C_α representation used in these methods is unable to capture these kinds of details. The average increase in correlation coefficients when using the FRI over GNM on the superset of 365 proteins is 0.096 for opFRI and 0.059 for pfFRI. Additionally, opFRI and pfFRI are more accurate on average than GNM and NMA for all three sets of structures used by Park et al.[28] From these results we conclude that both FRI and pfFRI are more accurate on average than either GNM or NMA.

III.C.2 fFRI vs GNM

Table 3: Average correlation coefficients (CC) of B-factor prediction for a set of 365 proteins using fFRI ($R = 12$). The improvements of the fFRI over the GNM prediction (0.565) are given in parentheses.

Exponential parameters	Avg. CC	Lorentz parameters	Avg. CC
κ=0.5, η=0.5	0.615 (8.8%)	υ=2.5, η=2.0	0.622 (10.1%)
κ=1.0, η=3.0	0.623 (10.3%)	υ=3.0, η=3.0	0.626 (10.8%)
κ=1.5, η=6.0	0.619 (9.6%)	υ=3.5, η=4.0	0.623 (10.3%)

Table 3 lists the average correlation coefficients of B-factor prediction for 365 proteins using fFRI schemes at a given truncation ($R = 12$Å). It is seen that the proposed fFRI schemes implemented in either exponential ($\eta = 3$Å and $\kappa = 1$) or Lorentz ($\eta = 3$Å and $\upsilon = 3$) are at least 10% more accurate than the GNM.

III.D Efficiency comparison for FRI, fFRI and GNM

This section concerns the computational efficiency of the FRI method. The efficiency of the FRI and the fFRI is compared with that of the GNM in this section.

Computational efficiency in the B-factor prediction becomes important for large proteins and for repeated predictions in molecular dynamics simulation and flexible docking analysis. High efficiency in the rigidity analysis is also a requirement for CEWAR dynamics, where atomic rigidity functions are to be evaluated during the time evolution. The previously described set of 44 proteins as listed in Table 8 are used to test the computational complexity of the FRI, fFRI and GNM algorithms. The method used to obtain the structure of the HIV virus capsid, which has more than 313,000 amino acid residues, does not provide experimental B-factors. To ensure a fair test, we have added some random noise to the predicted B-factors. The resulting B-factors of the HIV structure are employed in our efficiency test as if they were real experimental data.

Table 8 and Figure 4 are the running times for each method in our FORTRAN implementations of GNM and FRI. Tests were conducted using a single core of an AMD Phenom II X6 1100T processor and include the

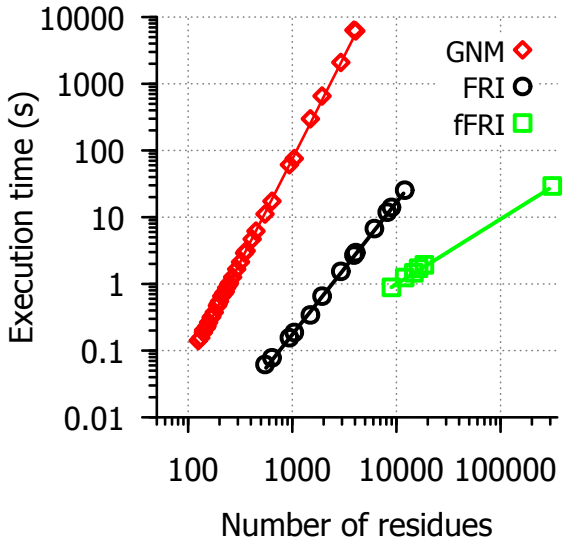

Figure 4: Efficiency comparison between FRI algorithms and GNM. Execution time in second (s) vs. number of residues for FRI (circle), fFRI (square) and GNM (diamond). A set of 44 C_α only PDB files was used to evaluate the computational complexity of GNM, FRI and fFRI. Available correlation coefficient values are listed in Table 8.

entire GNM and FRI algorithm leaving out only the time it takes to load PDB files. As expected, GNM has a computational complexity close to $\mathcal{O}(N^3)$ due to the matrix decomposition, while the FRI is approximately of $\mathcal{O}(N^2)$, mainly because of the computation of correlation functions. As for the fFRI, its computational complexity is of $\mathcal{O}(N)$ due to the nature of its sparse matrix. The lines of best fit for CPU time (t) are: $t = (4 \times 10^{-8}) * N^{3.09}$ for GNM, $t = (2 \times 10^{-7}) * N^{1.98}$ for FRI and $t = (1 \times 10^{-7}) * N^{0.975}$ for fFRI. Some of the 44 structures used for efficiency testing were excluded from the final analysis of the FRI and fFRI methods because they required so little time to run that it was not possible to get an accurate measure of execution time. A few of the largest structures were only tested with FRI and fFRI methods because they require much more CPU time to run with GNM and the efficiency data are already sufficient to show that GNM scales at approximately $\mathcal{O}(N^3)$. For a protein of seven thousand amino acid residues, it takes close to ten thousand seconds for GNM and only a few seconds for the FRI to predict the B-factors in our test. The fFRI is significantly faster than other methods. It takes less than 30 seconds for the fFRI to predict the B-factors of the HIV virus capsid with 313236 residues.

III.E Visualization of correlation maps

The correlation functions used to generate FRI correlation maps are based on monotonically decreasing radial basis functions. NMA, GNM and related tools, on the other hand, use either a Kirchhoff (i.e., contact matrix) or a cross correlation map for connectivity between atoms. A Kirchhoff matrix is similar to our correlation map except the values are set to -1 for pairs of atoms within a cutoff distance and set to 0 for pairs of atoms outside the cutoff distance. The downside of using the Kirchhoff matrix is that, by definition, it treats all bonds within a certain cutoff distance the same and neglects all interactions outside that distance. We know that the closest atoms, such as covalently bonded atoms, will contribute more to the rigidity of a particular atom. With a rapidly decaying distance function, such as those used in our correlation functions, the impact of covalently bonded atoms is emphasized over the interactions that are just slightly more distant. This relationship is important because while structural features at a distance can play a significant role in stability and flexibility of a molecule, local structure has a much greater impact. Additionally, the cross correlation map in GNM and other methods does not reflect the atomic distance relations in a direct manner. In contrast, given a correlation matrix and a function from the FRI method it is easy to reconstruct the position of each C_α atom in our coarse-grained model. The FRI correlation maps on the right side of Fig. 5 display distance values along side the correlation values to reflect this property of the FRI. These maps were calculated using the Lorentz function with υ=2.5. The second case (PDB: 1AIE), a single α-helix, is a good example of how the distance based correlation map reflects secondary structure information. The width of the band of high correlation is four amino acids, approximately the number of amino acids in one turn of an α-helix. For atoms within one turn of the helix, correlation values to nearby atoms follow a predictable pattern based on their distance. The cross-correlation matrix for 1AIE from GNM shows a

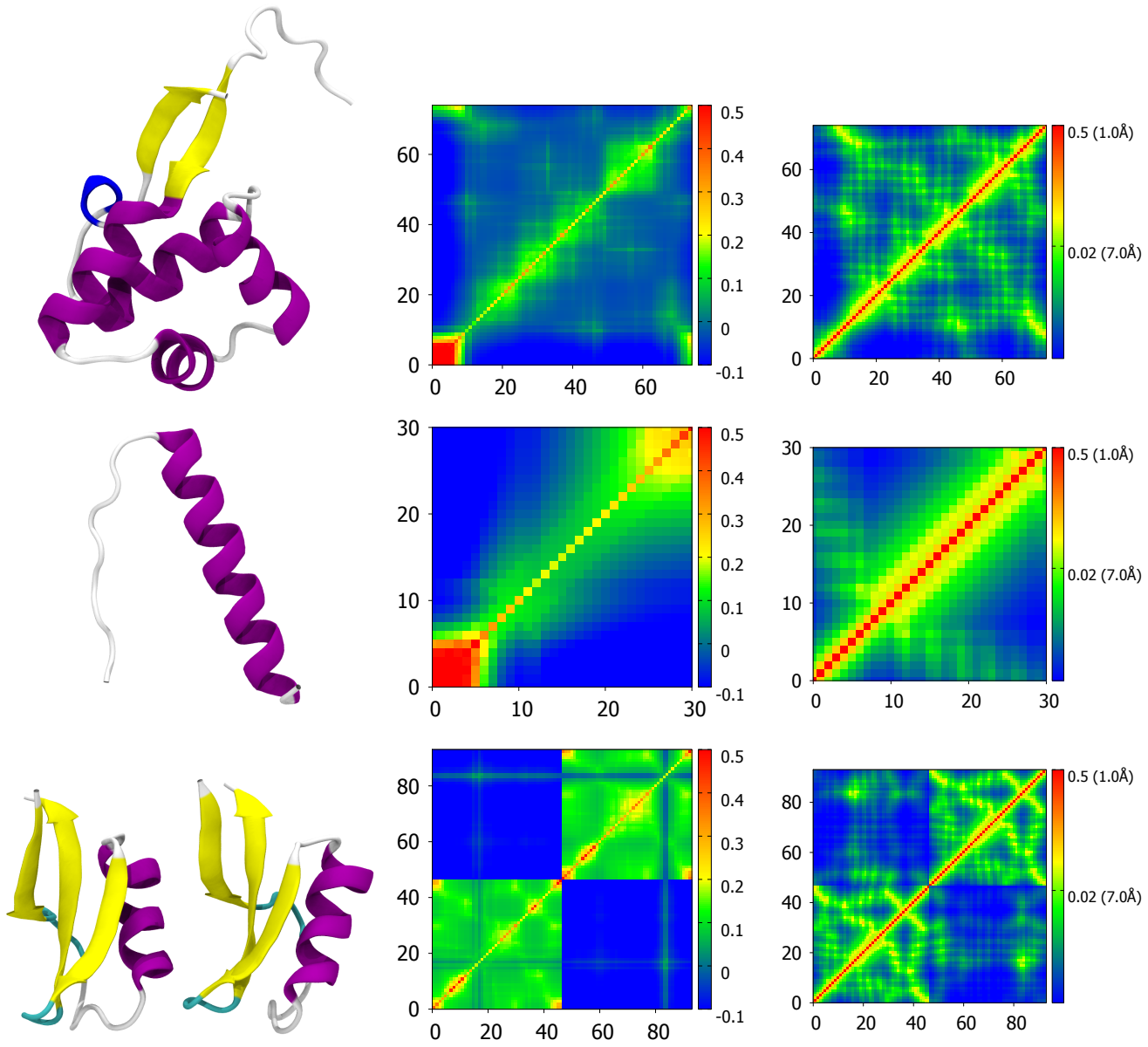

Figure 5: Comparison of correlation maps generated by GNM (middle) and FRI (right) for three proteins which are displayed in a secondary structure representation (left). From top to bottom, PDB IDs for the structures displayed are 3TYS, 1AIE and 3PSM. The three-dimensional representation of each protein is generated in VMD[18] and colored by secondary structure. The correlation maps in the middle column are computed using the GNM method and the correlation maps from the FRI method are shown in the right column.

similar overall pattern but without the same kind of atomic detail from the distance based correlation functions.

The other structures in Fig. 5 are from larger proteins and they show how the FRI and GNM represent complex arrangements of secondary structures. The FRI correlation maps clearly indicate where secondary structures are in the protein and what other residues they interact closely with. In these correlation maps, secondary structures are typically shown as small bands of relatively high correlation (yellow to red) while interactions between them appear in green and they often appear as regularly spaced green spots. These spots have space between them because they involve interactions with one face of an α-helix or similar fold and so the residues on the far side have a lower correlation. The cross-correlation matrix from GNM also gives some indication of where secondary structures are, α-helix is a square of green and beta sheets are lines, however these shapes are less defined on the atomic scale. Similarly the interactions between secondary structures are harder to pinpoint atomically as these interactions appear as a green smear in the matrices while in the correlation maps

of the FRI method there are discrete spots with individual correlation values for atom to atom interactions. In the last example of Fig. 5 we can also see in the top left and bottom right corners how each map displays the interaction between two images of a structure from a single X-ray crystallography experiment.

IV Protein domain analysis with FRI and aFRI

IV.A FRI for protein identification

Structural domains, as opposed to functional domains, are the basic unit of protein structures. Typically these portions of a protein fold independently and are stable on their own. The way various domains are assembled in a protein dictates its shape and function and is therefore interesting to biologists. One simple way to identify these domains and their interactions is by looking at the correlation matrix. The FRI correlation matrix or correlation map allows us to identify protein structural domains because the values of a correlation function directly reflect the pairwise distances between Cα-Cα atoms. Therefore FRI correlation maps are also distance maps, which have been shown to be an effective tool for identifying protein domains as early as 1974.[31] This method involves generating a Cα-Cα pairwise distance map and identifying dense, triangular areas of contacts near the diagonal. The correlation matrix generated for FRI is similar to a basic Cα-Cα distance map with the benefit of a rapidly decaying distance function. This results in more pronounced separation between domains in the map, potentially making it easier to identify distinct domains. Figure 6 demonstrates how domains are identified on a Cα-Cα distance map or a FRI correlation matrix for three proteins of increasing size and complexity. Each protein is divided into two structural domains outlined with red boxes for clarity.

In more complex cases, we see larger domains made up of multiple subdomains. Figure 7 shows the HIV capsid protein (PDB ID: 1E6J) consisting of six distinct structural domains. Alongside the protein's secondary structure are the contact matrix used in GNM and the correlation maps from the FRI. By adjusting the distance cutoff in the GNM and correlation function parameters in the FRI we arrive at similar results. The six compact structural subdomains can be identified visually from these matrices by finding areas with high correlation or large numbers of contacts in a triangular shape near the diagonal. Some interactions between subdomains can also be seen in the matrices. Subdomains with a significant level of correlation or contacts between them can be considered as single larger domain. In the example of Figure 7, there are contacts in the matrices between five subdomains. The last subunit (green color) shows little or no correlation or contacts to the other subdomains and is therefor a separate domain and expected to move fully independently. However, predicting domain motions with the FRI requires an alternative formulation, the anisotropic FRI.

IV.B aFRI for protein identification

Anisotropic FRI, like ANM, predicts the amplitudes and directions of atomic fluctuations. To test the accuracy of this new method we can compare aFRI fluctuation predictions to experimental B-factors as we have done with FRI and GNM. Both anisotropic rigidity based flexibility (f_i^{AR}) and anisotropic flexibility based flexibility (f_i^{AF}) are examined for their B-factor predictions and their average correlation coefficients are 0.602 ($\upsilon = 2$ and $\eta = 9$) and 0.572 ($\upsilon = 2$ and $\eta = 18$) for the superset of 365 structures. This means that aFRI is more accurate than GNM (average correlation coefficient 0.565 for the superset). However, aFRI is slightly less accurate than pfFRI (average correlation coefficient 0.626 for the superset), which is similar to the fact that ANM is not as accurate as GNM.

A major utility of the proposed aFRI theory is the prediction of protein motions by using the anisotropic flexibility. Since aFRI is adaptive, its cluster can be as large as the whole molecule and as small as a single particle. The completely global aFRI has a Hessian matrix of $3N \times 3N$ elements and produces $3N$ eigenmodes. Depending on symmetry, 5 or 6 modes are due to the translational and rotational motions. Therefore, the remaining $3N - 5$ or $3N - 6$ vibrational modes can be obtained. To validate the proposed aFRI theory for normal mode analysis, we have computed the vibrational modes for a few simple molecules, namely, H_2O, CO_2 and CH_2O, whose vibrational modes are well-known. Our results are displayed in Figure 8. In addition to these vibrational modes, appropriate translational and rotational modes are also observed from our calculations, but are omitted in our presentation. Therefore, the proposed aFRI works well for the analysis of small molecular translation, rotation, and vibration.

Having established our aFRI for small molecular vibrational analysis, we are interested in examining its behavior for macromolecules. Anisotropic normal mode analysis of large biomolecules can be very expensive because the computational complexity of the global matrix scales as $\mathcal{O}((3N)^3)$. As such, the adaptive cluster analysis option provided by the aFRI algorithm can be useful. In this work, we explore two extreme aFRI options, i.e., the completely global cluster and completely local clusters, for protein vibrational analysis. Similar to the ANM, the completely global aFRI algorithm has a Hessian matrix of $3N \times 3N$ elements and produces $3N$ eigenmodes.

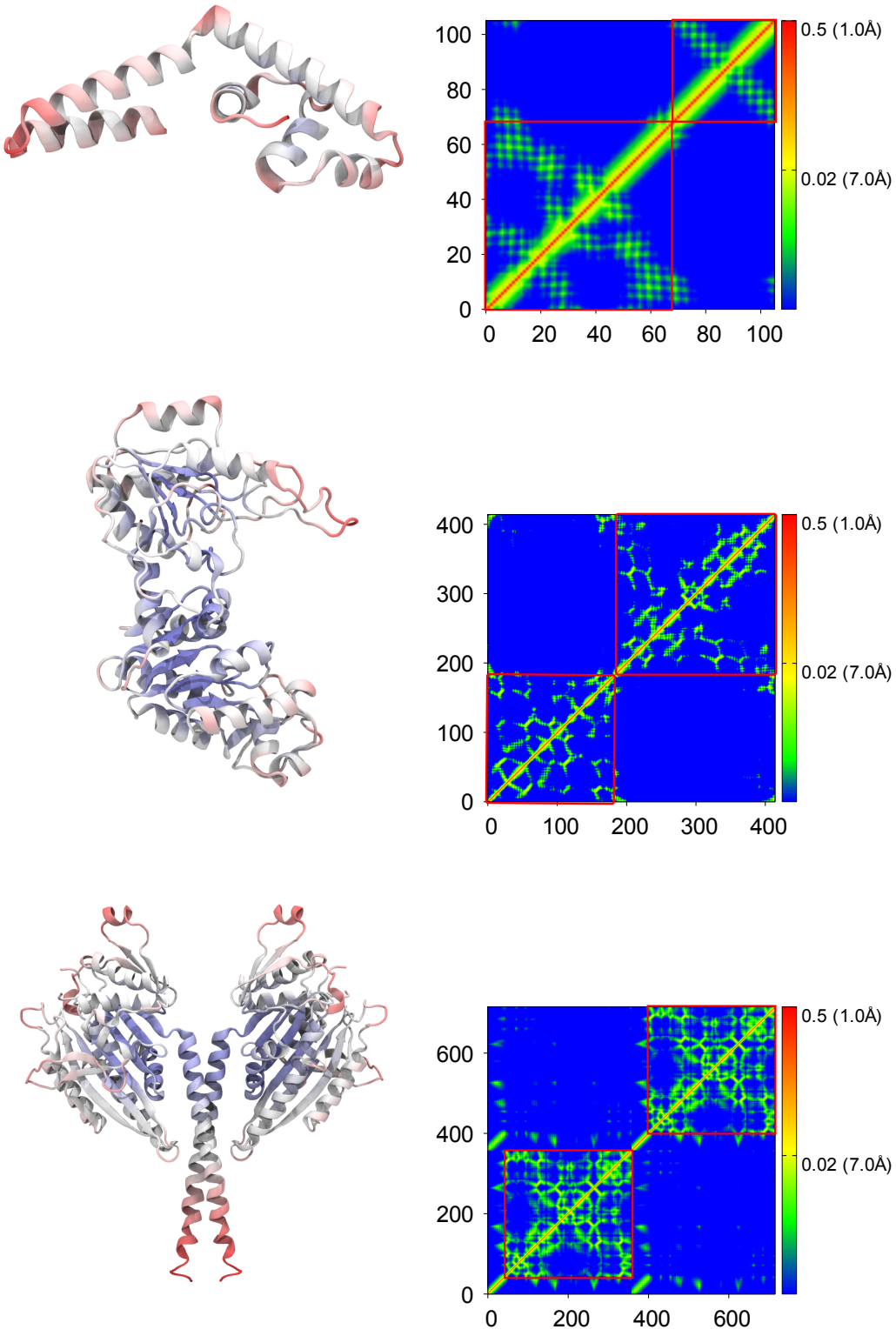

Figure 6: Secondary structure representations and correlation maps for PDB structures 1S7O, 3PGK and 2NCD. Structures colored by values of the correlation function of the FRI using the exponential function with κ=0.4 and η=0.8Å, which are the optimal values for 2NCD kinesin with a correlation coefficient of 0.671. All three-dimensional images are rendered using VMD.[18]

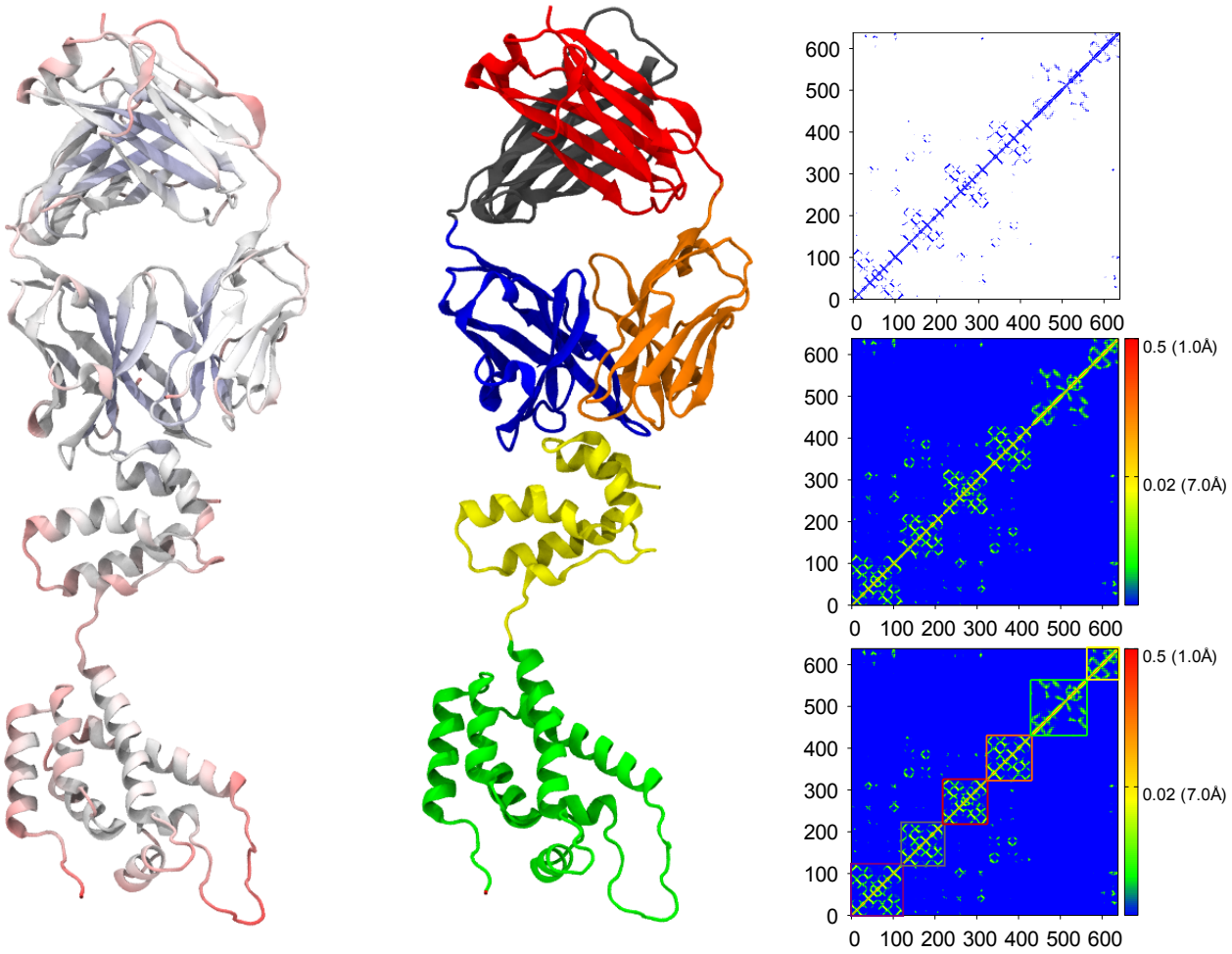

Figure 7: HIV capsid protein secondary structures (left and middle) and contact matrix from GNM (top right) and correlation matrix from FRI (middle right and bottom right). Secondary structure representations are colored by flexibility from FRI (left) and by domain (middle). Domain separations are highlighted in color coded boxes in the FRI correlation matrix at bottom right. All three-dimensional images are rendered using VMD.[18]

The motions predicted by these eigenmodes are typically very similar to those produced by ANM. In contrast, the completely localized aFRI has only a total of N 3×3 Hessian matrices and gives rise to $3N$ eigenmodes for N particles. We assemble these $3N$ eigenmodes into 3 modes for the molecule and weight the amplitude of each eigenmode by the corresponding B-factor for the particle. Due to the non-local correlation built in the aFRI matrices, these three modes of motion obtained by the completely local aFRI algorithm are often similar to certain low-order modes calculated by ANM for a protein. The first three modes of motion for the HIV capsid protein are shown in Figure 9 for two aFRI algorithms and ANM. It is seen that three eigenmodes obtained from the completely global aFRI resemble those calculated by the ANM. Although three modes produced by the completely local aFRI algorithm show different motions, it is amazing to note that there is much collective motion in these modes.

Figure 10 depicts three modes for phosphate active transport receptor protein generated by using two aFRI algorithms and ANM. Once again, we see a good similarity between eigenmodes calculated by using the completely global aFRI algorithm and those computed by using the ANM. However, the modes generated with the completely localized aFRI demonstrate somewhat different motions. In each method, the relative motion of two domains can be clearly identified. The domain relative motions in the eigenmodes of the completely global aFRI and the ANM exhibit a better synergistic effect in general. Whereas, modes from the completely local aFRI are slightly less collective. Since there is no standard answer to domain fluctuations, it is difficult to say which one is right or wrong. An interesting observation is that although aFRI matrices can be completely local, they have

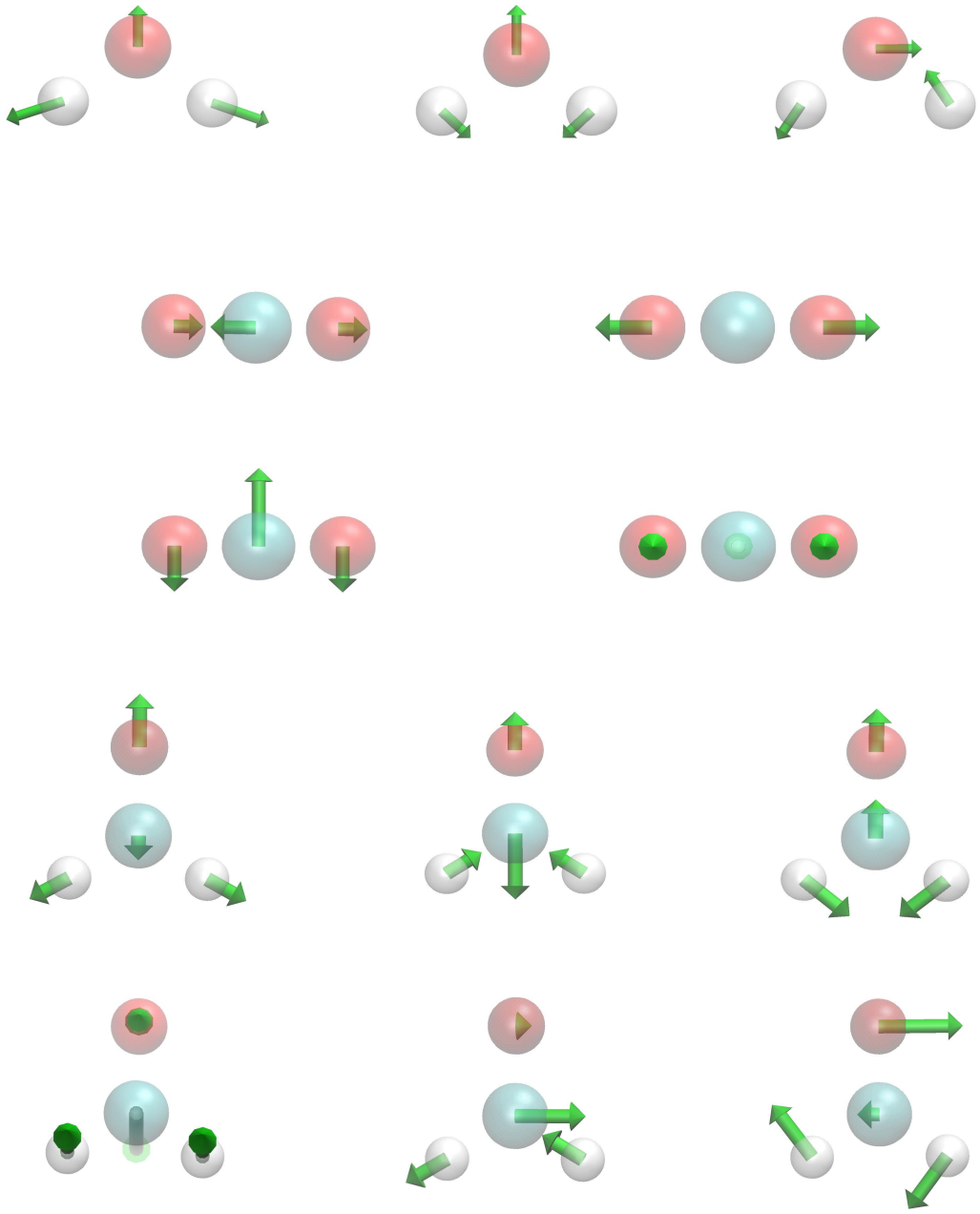

Figure 8: Validation of the completely global aFRI for the vibrational analysis of three small molecules ($\upsilon = 2$). First row: three vibrational modes for H_2O ($\eta = 1$); Second and third rows: four vibrational modes for CO_2 ($\eta = 1$); Last two rows: six vibrational modes for CH_2O ($\eta = 2$). All three-dimensional images are rendered using VMD.[18]

built in non-local correlation and thus are able to simulate highly collective protein motions.

V Concluding remarks

The fundamental challenges that hinder the current quantitative understanding of biomolecular systems are their tremendous complexity and excessively large number of degrees of freedom. A multiscale approach, the continuum elasticity with atomic rigidity (CEWAR), provides a new method for the reduction of the number of degrees of freedom in biomolecular systems.[46] The performance of the CEWAR method relies on the accurate

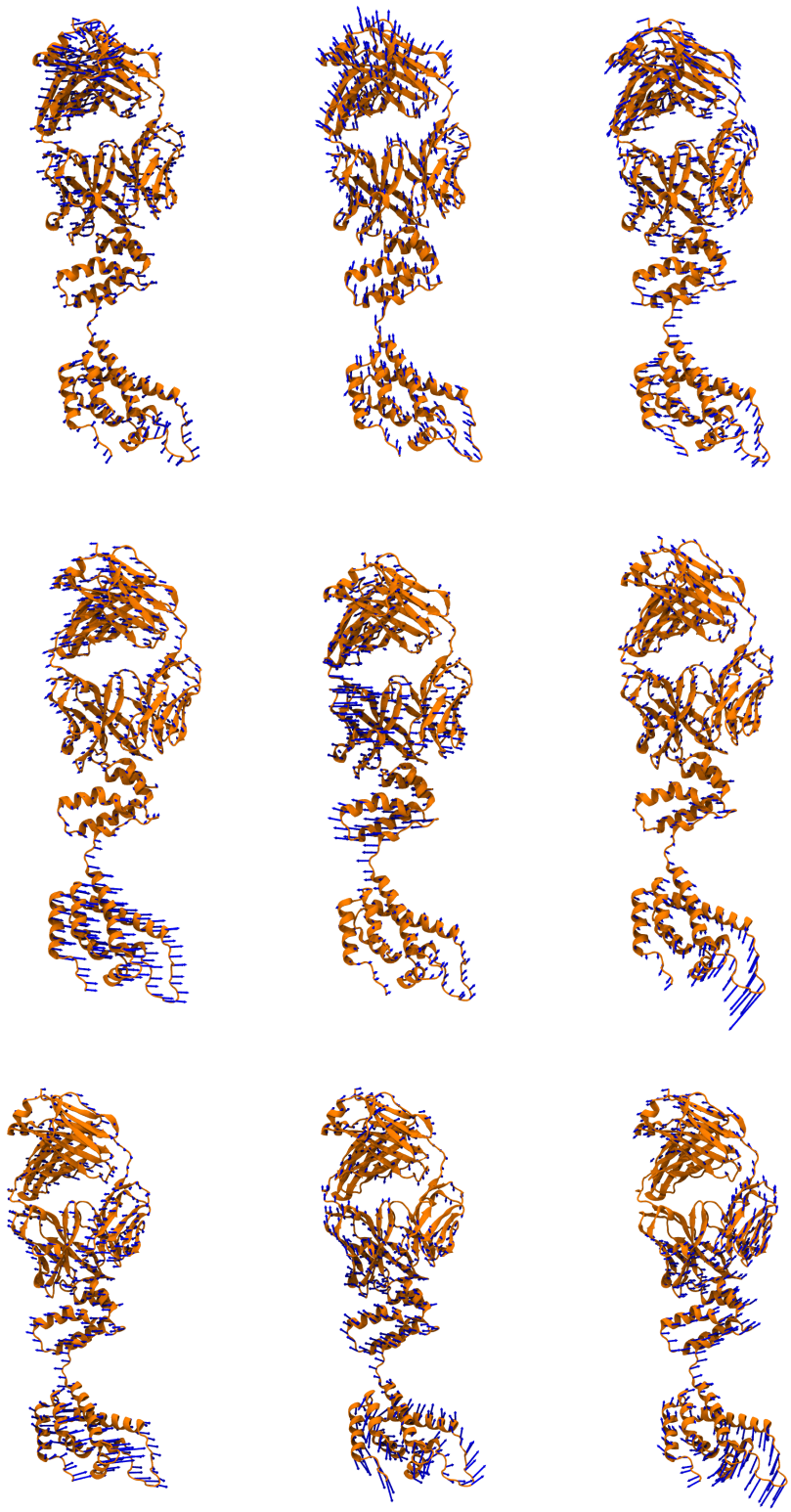

Figure 9: Comparison of modes for HIV capsid protein (PDB ID: 1E6J). The top row is generated by using the completely local aFRI with $\upsilon = 2$ and $\eta = 50$. The middle row is generated by using the completely global aFRI with $\upsilon = 2$ and $\eta = 50$. The bottom row is generated by using the ANM with ProDy v1.5[6] using default settings. All three-dimensional images are rendered using VMD.[18]

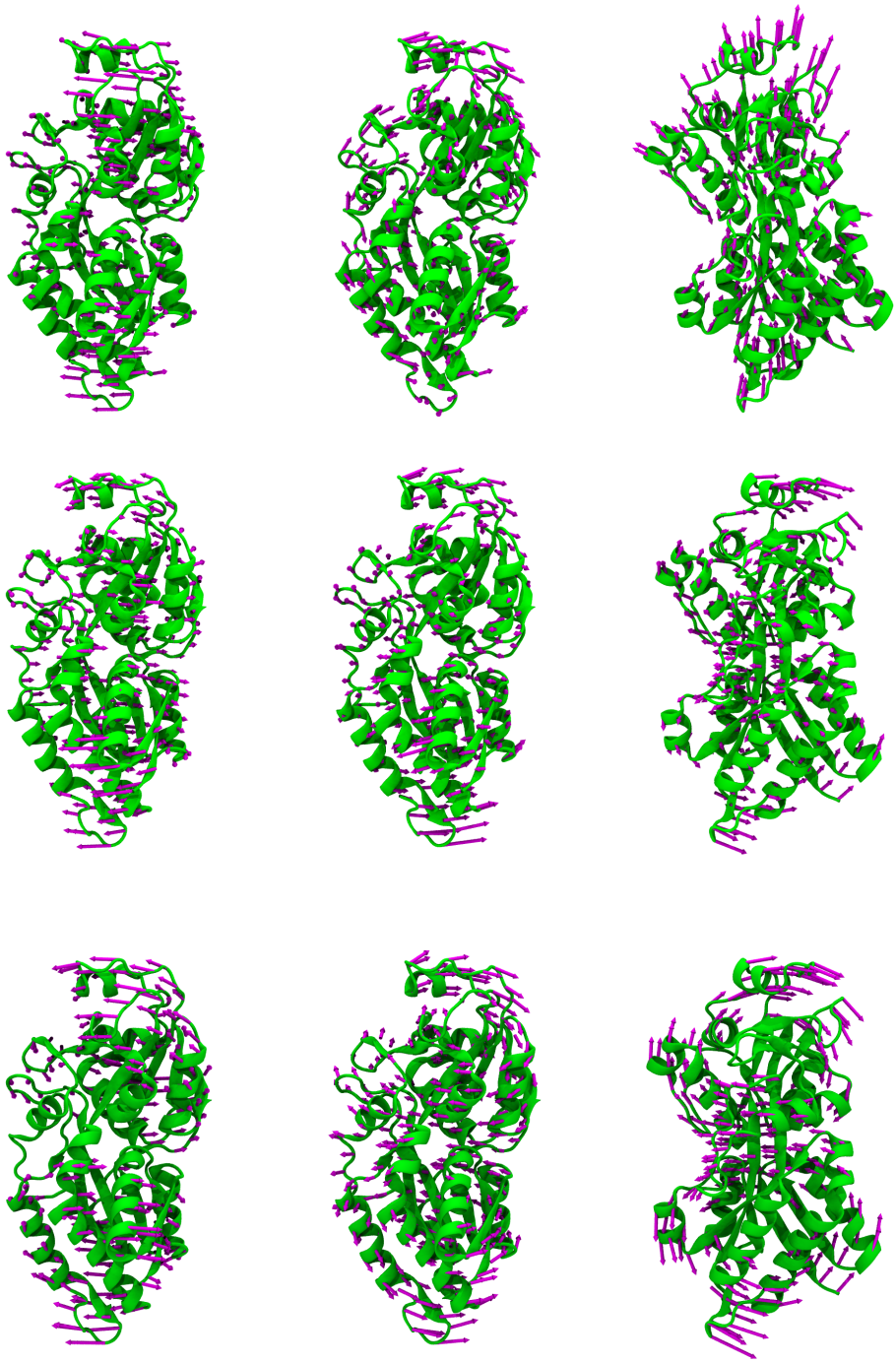

Figure 10: Comparison of modes for phosphate active transport protein (PDB ID: 2ABH). The top row is generated by using the completely local aFRI with $\upsilon = 2$ and $\eta = 60$. The middle row is generated by using the completely global aFRI with $\upsilon = 2$ and $\eta = 35$. The bottom row is generated by using the ANM with ProDy v1.5[6] using default settings. All three-dimensional images are rendered using VMD.[18]

and efficient evaluation of a continuous atomic rigidity function. The flexibility-rigidity index (FRI) is proposed as a potential algorithm for such an evaluation. The underlying assumption of the FRI is that protein interactions uniquely determine the protein structure which, in turn, determines the protein functions, such as stability and flexibility. Therefore, one just needs the structural information to predict protein B-factors without reconstructing the protein interaction Hamiltonian. In particular, we assume that biomolecular flexibility and rigidity are local

structural properties. Therefore, the flexibility at an atom is completely determined by its local environment, namely, local geometry and local topological connectivity. We treat the (local) flexibility as an inverse of the (local) rigidity. As a consequence, we do not need to solve the (global) eigenvalue problem of the Hamiltonian. The first step of the FRI method is to measure protein topological connectivity from the distance geometry via smooth and monotonically decreasing radial basis functions. The atomic rigidity index is then associated with the total connectivity or interaction strength at each residue. Consequently, the atomic flexibility index, which is the inverse function of the atomic rigidity index, is associated with protein B-factors.

Protein flexibility is an intrinsic property that strongly correlates with protein functions. The analysis of protein flexibility is a crucial task in computational biophysics. Many established methods, including normal mode analysis (NMA)[7,15,23,39] and elastic network model (ENM)[41] such as Gaussian network model (GNM),[4,5,12] have been developed in the past. These approaches typically depend on the Hamiltonian mechanics of elastic interactions and matrix decomposition of the interaction Hamiltonian. The present work examines the performance of the proposed FRI for protein flexibility analysis in a comparison with some cutting edge methods, specifically, GNM and NMA.

We calibrate the accuracy, reliability and computational efficiency of the FRI method by using GNM and NMA on three sets of proteins, i.e, relatively small-sized, medium sized and large sized structures employed by Park et al.[28] in a recent study. Additional calibration with the GNM is carried out on extended set. As a result, a total of 365 proteins is studied in the present comparative study. As an internal validation, the FRI method is realized by using three families of correlation functions. Correlation functions of generalized exponential type and Lorentz type are found to deliver better results. In particular, correlation functions of Lorentz type are simple and can be made parameter free, which is desirable for general use. Although GNM and NMA may outperform the proposed FRI method on certain proteins in terms of the accuracy of the B-factor prediction, the FRI method is able to improve on the average correlation coefficient of GNM and NMA on all three sets of proteins. Additionally, the FRI is found to significantly outperform the GNM on the extended superset of 365 structures as well.

A possible reason for the FRI to outperform the existing methods is that GNM and NMA are essentially global methods in a sense that they rely on the solution of the global eigenvalue problem to predict local atomic properties, e.g., B-factors. In contrast, the FRI is a local method and utilizes the local geometric information to predict local atomic properties. In parallel, there are (global) band theory of solids and (local) atomic orbital model of solids. The former is good for describing many global physical properties, such as electrical conductivity and thermal lattice motions in terms of excitations, while the latter is more powerful for explaining localized chemical reactivity and catalysis of solids.

The GNM is known for its superb computational efficiency.[48] The matrix diagonalization is of $\mathcal{O}(N^3)$ in computational complexity, where N is the number of residues. The computational complexity of our original FRI is of $\mathcal{O}(N^2)$. In the present work, we propose a fast FRI (fFRI) algorithm, which further reduces the computational complexity of FRI to $\mathcal{O}(N)$. Both FRI and fFRI do not involve the time consuming matrix decomposition. As a result, it takes less than 30 seconds for the fFRI to predict the B Factors of an HIV virus structure with more than three hundred thousands of residues, which otherwise requires many years for the GNM to compute. Additionally, both the exponential based parameter-free fFRI and the Lorentz based parameter-free fFRI are about 10% more accurate than the GNM in the B-factor prediction of 365 proteins.

Anisotropic motions between protein domains are known to correlate with protein functions. To describe protein anisotropic fluctuations, we introduce anisotropic FRI (aFRI) algorithms. We introduce an adaptive aFRI method which partitions the molecule into many clusters with variable sizes. We specifically examine two extreme cases, i.e., a one-cluster partition and N-cluster partition, which result in a completely global $3N \times 3N$ Hessian matrix and N completely localized 3×3 Hessian matrices, respectively. The computational complexity of aFRI varies from $\mathcal{O}(N^3)$ to $\mathcal{O}(N)$. Although aFRI Hessian matrices can be completely local, they still contain much non-location correlation. As such, all of three protein modes predicted by the completely local aFRI exhibit highly collective global motions. The eigenmodes obtained from the completely global aFRI closely resemble those of the anisotropic network model (ANM).[3,6] However, mode constructed from the completely local aFRI show different collective motion patterns. Since there is no analytical solution for collective motions, it is not possible to judge whose collective motions are more correct. In general, the eigenmodes of ANM and the completely global aFRI exhibit a slightly better synergistic effect than modes generated by using the completely local aFRI.

The proposed FRI has a few visual applications. First, the correlation maps of the FRI are capable of revealing both short- and long-distance interactions or connectivities. Since correlation map elements are directly related to the original distances by a known radial basis function, the distances can be labeled on the map as well.

Additionally, the predicted B-factors can be plotted as the radii of residues to visualize the amplitude of thermal fluctuations. This plot becomes even more interesting when atomic spheres are colored with the electrostatics.[46] The close correlation between flexibility and large electrostatic potentials can be unveiled, which sheds light on protein intrinsic structural properties. Moreover, the predicted B-factors can be plotted with secondary structures to have an overall picture of structural flexibility. Finally, as continuous functions, the atomic rigidity function and atomic flexibility function can be projected onto protein molecular surfaces or other surface representations to analyze flexibility.

Another application of FRI and aFRI is the analysis of protein domains. Existing methods, such as GNM and ANM, are well known to do well for domain analysis. The present FRI provides a clear correlation map for domain identifications. It is found that aFRI gives rise to highly collective domain motion patterns, although not all parts of a domain move uniformly in our aFRI representations.

Acknowledgments

This work was supported in part by NSF grants IIS-1302285 and DMS-1160352, NIH grant R01GM-090208 and MSU Center for Mathematical Molecular Biosciences Initiative. KO thanks Dr Minxin Chen for useful discussion about the data structure of cell lists. The authors acknowledge the Mathematical Biosciences Institute for hosting valuable workshops.

References

[1] M. P. Allen and D. J. Tildesley. *Computer Simulation of Liquids*. Oxford: Clarendon Press, 1987.

[2] C. B. Anfinsen. Einfluss der configuration auf die wirkung den. *Science*, 181:223 – 230, 1973.

[3] A. R. Atilgan, S. R. Durrell, R. L. Jernigan, M. C. Demirel, O. Keskin, and I. Bahar. Anisotropy of fluctuation dynamics of proteins with an elastic network model. *Biophys. J.*, 80:505 – 515, 2001.

[4] I. Bahar, A. R. Atilgan, M. C. Demirel, and B. Erman. Vibrational dynamics of proteins: Significance of slow and fast modes in relation to function and stability. *Phys. Rev. Lett*, 80:2733 – 2736, 1998.

[5] I. Bahar, A. R. Atilgan, and B. Erman. Direct evaluation of thermal fluctuations in proteins using a single-parameter harmonic potential. *Folding and Design*, 2:173 – 181, 1997.

[6] A. Bakan, L. M. Meireles, and I. Bahar. Prody: Protein dynamics inferred from theory and experiments. *Bioinformatics*, 27:1575 –1577, 2011.

[7] B. R. Brooks, R. E. Bruccoleri, B. D. Olafson, D. States, S. Swaminathan, and M. Karplus. Charmm: A program for macromolecular energy, minimization, and dynamics calculations. *J. Comput. Chem.*, 4:187–217, 1983.

[8] F. Chiti and C. M. Dobson. Protein misfolding, functional amyloid, and human disease. *Annu. Rev. Biochem.*, 75:333 – 366, 2006.

[9] Q. Cui and I. Bahar. *Normal mode analysis: theory and applications to biological and chemical systems*. Chapman and Hall/CRC, 2010.

[10] Q. Cui, G. J. Li, J. Ma, and M. Karplus. A normal mode analysis of structural plasticity in the biomolecular motor f(1)-atpase. *J. Mol. Biol.*, 340(2):345 – 372, 2004.

[11] O. N. A. Demerdash and J. C. Mitchell. Density-cluster NMA: A new protein decomposition technique for coarse-grained normal mode analysis. *Proteins:Structure Function and Bioinformatics*, 80(7):1766–1779, JUL 2012.

[12] P. J. Flory. Statistical thermodynamics of random networks. *Proc. Roy. Soc. Lond. A,*, 351:351 – 378, 1976.

[13] H. Frauenfelder, S. G. Slihar, and P. G. Wolynes. The energy landsapes and motion of proteins . *Science*, 254(5038):1598–1603, DEC 13 1991.

[14] Z. N. Gerek and S. B. Ozkan. A flexible docking scheme to explore the binding selectivity of pdz domains. *Protein Science*, 19:914–928, 2010.

[15] N. Go, T. Noguti, and T. Nishikawa. Dynamics of a small globular protein in terms of low-frequency vibrational modes. *Proc. Natl. Acad. Sci.*, 80:3696 – 3700, 1983.

[16] K. Hinsen. Analysis of domain motions by approximate normal mode calculations. *Proteins*, 33:417 – 429, 1998.

[17] K. Hinsen. Structural flexibility in proteins: impact of the crystal environment. *Bioinformatics*, 24:521 – 528, 2008.

[18] W. Humphrey, A. Dalke, and K. Schulten. VMD – visual molecular dynamics. *Journal of Molecular Graphics*, 14(1):33–38, 1996.

[19] D. J. Jacobs, A. J. Rader, L. A. Kuhn, and M. F. Thorpe. Protein flexibility predictions using graph theory. *Proteins-Structure, Function, and Genetics*, 44(2):150–165, AUG 1 2001.

[20] O. Keskin, I. Bahar, D. Flatow, D. G. Covell, and R. L. Jernigan. Molecular mechanisms of chaperonin groel-groes function. *Biochem.*, 41:491 – 501, 2002.

[21] D. A. Kondrashov, A. W. Van Wynsberghe, R. M. Bannen, Q. Cui, and J. G. N. Phillips. Protein structural variation in computational models and crystallographic data. *Structure*, 15:169 – 177, 2007.

[22] S. Kundu, J. S. Melton, D. C. Sorensen, and J. G. N. Phillips. Dynamics of proteins in crystals: comparison of experiment with simple models. *Biophys. J.*, 83:723 – 732, 2002.

[23] M. Levitt, C. Sander, and P. S. Stern. Protein normal-mode dynamics: Trypsin inhibitor, crambin, ribonuclease and lysozyme. *J. Mol. Biol.*, 181(3):423 – 447, 1985.

[24] G. H. Li and Q. Cui. A coarse-grained normal mode approach for macromolecules: an efficient implementation and application to Ca(2+)-ATPase. *Bipohys. J.*, 83:2457 – 2474, 2002.

[25] D. R. Livesay, S. Dallakyan, G. G. Wood, and D. J. Jacobs. A flexible approach for understanding protein stability. *FEBS Letters*, 576:468–476, 2004.

[26] J. P. Ma. Usefulness and limitations of normal mode analysis in modeling dynamics of biomolecular complexes. *Structure*, 13:373 – 180, 2005.

[27] J. N. Onuchic, Z. Luthey-Schulten, and P. G. Wolynes. Theory of protein folding: The energy landscape perspective. *Annu. Rev. Phys. Chem*, 48:545–600, 1997.

[28] J. K. Park, R. Jernigan, and Z. Wu. Coarse grained normal mode analysis vs. refined gaussian network model for protein residue-level structural fluctuations. *Bulletin of Mathematical Biology*, 75:124 –160, 2013.

[29] A. J. Rader, D. H. Vlad, and I. Bahar. Maturation dynamics of bacteriophage hk97 capsid. *Structure*, 13:413 – 421, 2005.

[30] R. J. Renka. Multivariate interpolation of large sets of scattered data. *ACM Transactions on Mathematical Software*, 14(2):139–148, JUN 1988.

[31] M. G. Rossman and A. Liljas. Recognition of structural domains in globular proteins. *Journal of Molecular Biology*, 85:177âĂŞ181, 1974.

[32] M. Schroder and R. J. Kaufman. The mammalian unfolded protein response. *Annual Review of Biochemistry*, 74:739 – 789, 2005.

[33] D. Sept and F. C. MacKintosh. Microtubule Elasticity: Connecting All-Atom Simulations with Continuum Mechanics. *Physical Review Letters*, 104(1), Jan 8 2010.

[34] L. Skjaerven, S. M. Hollup, and N. Reuter. Normal mode analysis for proteins. *Journal of Molecular Structure: Theochem.*, 898:42 – 48, 2009.

[35] G. Song and R. L. Jernigan. vgnm: a better model for understanding the dynamics of proteins in crystals. *J. Mol. Biol.*, 369(3):880 – 893, 2007.

[36] F. Tama and C. K. Brooks III. Diversity and identity of mechanical properties of icosahedral viral capsids studied with elastic network normal mode analysis. *J. Mol. Biol.*, 345:299 – 314, 2005.

[37] F. Tama and Y. H. Sanejouand. Conformational change of proteins arising from normal mode calculations. *Protein Eng.*, 14:1 – 6, 2001.

[38] F. Tama, M. Valle, J. Frank, and C. K. Brooks III. Dynamic reorganization of the functionally active ribosome explored by normal mode analysis and cryo-electron microscopy. *Proc. Natl Acad. Sci.*, 100(16):9319 – 9323, 2003.

[39] M. Tasumi, H. Takenchi, S. Ataka, A. M. Dwidedi, and S. Krimm. Normal vibrations of proteins: Glucagon. *Biopolymers*, 21:711 – 714, 1982.

[40] W. I. Thacker, J. Zhang, L. T. Watson, J. B. Birch, M. A. Iyer, and M. W. Berry. Algorithm 905: SHEPPACK: Modified Shepard Algorithm for Interpolation of Scattered Multivariate Data. *ACM Transactions on Mathematical Software*, 37(3), SEP 2010.

[41] M. M. Tirion. Large amplitude elastic motions in proteins from a single-parameter, atomic analysis. *Phys. Rev. Lett.*, 77:1905 – 1908, 1996.

[42] C. W. von der Lieth, K. Stumpf-Nothof, and U. Prior. A bond flexibility index derived from the constitution of molecules. *Journal of Chemical Information and Computer Science*, 36:711–716, 1996.

[43] Y. Wang, A. J. Rader, I. Bahar, and R. L. Jernigan. Global ribosome motions revealed with elastic network model. *J. Struct. Biol.*, 147:302 – 314, 2004.

[44] G. W. Wei. Wavelets generated by using discrete singular convolution kernels. *Journal of Physics A: Mathematical and General*, 33:8577 – 8596, 2000.

[45] S. H. White and W. C. Wimley. Membrane protein folding and stability: Physical principles. *Annual Review of Biophysics and Biomolecular Structure*, 28:319–365, 1999.

[46] K. L. Xia, K. Opron, and G. W. Wei. Multiscale multiphysics and multidomain models — Flexibility and rigidity. *Journal of Chemical Physics*, 139:194109, 2013.

[47] C. Xu, D. Tobi, and I. Bahar. Allosteric changes in protein structure computed by a simple mechanical model: hemoglobin t <–> r2 transition. *J. Mol. Biol.*, 333:153 – 168, 2003.

[48] L. W. Yang and C. P. Chng. Coarse-grained models reveal functional dynamics–i. elastic network models–theories, comparisons and perspectives. *Bioinformatics and Biology Insights*, 2:25 – 45, 2008.

[49] W. Zheng, B. R. Brooks, and D. Thirumalai. Allosteric transitions in the chaperonin groel are captured by a dominant normal mode that is most robust to sequence variations. *Biophys. J.*, 93:2289 – 2299, 2007.

[50] W. J. Zheng and S. Doniach. A comparative study of motor-protein motions by using a simple elastic-network model. *Proc. Natl. Acad. Sci. USA.*, 100(23):13253 – 13258, 2003.

Efficiency or accuracy results for five sets of proteins

Table 4: Correlation coefficients for B-factor prediction obtained by optimal FRI (opFRI), parameter free FRI (pfFRI) and Gaussian normal mode (GNM) for small-size structures. †GNM and NMA values are taken from the coarse-grained (Cα) GNM and NMA results reported in Park et al.[28] except where starred (*). Starred values indicate correlation coefficients, from our own test of GNM, that have significantly increased compared to the values reported by Park et al.[28] See Section III.C for details regarding the calculation of new GNM scores.

PDB ID	N	opFRI	pfFRI	GNM †	NMA †
1AIE	31	0.588	0.416	0.155	0.712
1AKG	16	0.373	0.350	0.185	-0.229
1BX7	51	0.726	0.623	0.706	0.868
1ETL	12	0.710	0.609	0.628	0.355
1ETM	12	0.544	0.393	0.432	0.027
1ETN	12	0.089	0.023	-0.274	-0.537
1FF4	65	0.718	0.613	0.674	0.555
1GK7	39	0.845	0.773	0.821	0.822
1GVD	52	0.781	0.732	0.591	0.570
1HJE	13	0.811	0.686	0.616	0.562
1KYC	15	0.796	0.763	0.754	0.784
1NOT	13	0.746	0.622	0.523	0.567
1O06	20	0.910	0.874	0.844	0.900
1OB4	16	0.776	0.763	0.750*	0.930
1OB7	16	0.737	0.545	0.652*	0.952
1P9I	29	0.754	0.742	0.625	0.603
1PEF	18	0.888	0.826	0.808	0.888
1PEN	16	0.516	0.465	0.270	0.056
1Q9B	43	0.746	0.726	0.656	0.646
1RJU	36	0.517	0.447	0.431	0.235
1U06	55	0.474	0.429	0.434	0.377
1UOY	64	0.713	0.653	0.671	0.628
1USE	40	0.438	0.146	-0.142	-0.399
1VRZ	21	0.792	0.695	0.677*	-0.203
1XY2	8	0.619	0.570	0.562	0.458
1YJO	6	0.375	0.333	0.434	0.445
1YZM	46	0.842	0.834	0.901	0.939
2DSX	52	0.337	0.333	0.127	0.433
2JKU	35	0.805	0.695	0.656	0.850
2NLS	36	0.605	0.559	0.530	0.088
2OL9	6	0.909	0.904	0.689	0.886
2OLX	4	0.917	0.888	0.885	0.776
6RXN	45	0.614	0.574	0.594	0.304

Table 5: Correlation coefficients for B-factor prediction obtained by optimal FRI (opFRI), parameter free FRI (pfFRI) and Gaussian normal mode (GNM) for medium-size structures. †GNM and NMA values are taken from the coarse-grained ($C\alpha$) GNM and NMA results reported in Park et al.[28] except where starred (*). Starred values indicate correlation coefficients, from our own test of GNM, that have significantly increased compared to the values reported by Park et al.[28] See Section III.C for details regarding the calculation of new GNM scores.

PDB ID	N	opFRI	pfFRI	GNM †	NMA †
1ABA	87	0.727	0.698	0.613	0.057
1CYO	88	0.751	0.702	0.741	0.774
1FK5	93	0.590	0.568	0.485	0.362
1GXU	88	0.748	0.634	0.421	0.581
1I71	83	0.549	0.516	0.549	0.380
1LR7	73	0.679	0.657	0.620	0.795
1N7E	95	0.651	0.609	0.497	0.385
1NNX	93	0.795	0.789	0.631	0.517
1NOA	113	0.622	0.604	0.615	0.485
1OPD	85	0.555	0.409	0.398	0.796
1QAU	112	0.678	0.672	0.620	0.533
1R7J	90	0.789	0.621	0.368	0.078
1UHA	83	0.726	0.665	0.638*	0.308
1ULR	87	0.639	0.594	0.495	0.223
1USM	77	0.832	0.809	0.798	0.780
1V05	96	0.629	0.599	0.632	0.389
1W2L	97	0.691	0.564	0.397	0.432
1X3O	80	0.600	0.559	0.654	0.453
1Z21	96	0.662	0.638	0.433	0.289
1ZVA	75	0.756	0.579	0.690	0.579
2BF9	36	0.606	0.554	0.680*	0.521
2BRF	100	0.795	0.764	0.710	0.535
2CE0	99	0.706	0.598	0.529	0.628
2E3H	81	0.692	0.682	0.605	0.632
2EAQ	89	0.753	0.690	0.695	0.688
2EHS	75	0.720	0.713	0.747	0.565
2FQ3	85	0.719	0.692	0.348	0.508
2IP6	87	0.654	0.578	0.572	0.826
2MCM	113	0.789	0.713	0.639	0.643
2NUH	104	0.835	0.691	0.771	0.685
2PKT	93	0.162	0.003	-0.193*	-0.165
2PLT	99	0.508	0.484	0.509*	0.187
2QJL	99	0.594	0.584	0.594	0.497
2RB8	93	0.727	0.614	0.517	0.485
3BZQ	99	0.532	0.516	0.466	0.351
5CYT	103	0.441	0.421	0.331	0.102

Table 6: Correlation coefficients for B-factor prediction obtained by optimal FRI (opFRI), parameter free FRI (pfFRI) and Gaussian normal mode (GNM) for large-size structures. †GNM and NMA values are taken from the coarse-grained (Cα) GNM and NMA results reported in Park et al.[28] except where starred (*). Starred values indicate correlation coefficients, from our own test of GNM, that have significantly increased compared to the values reported by Park et al.[28] See Section III.C for details regarding the calculation of new GNM scores.

PDB ID	N	opFRI	pfFRI	GNM †	NMA †
1AHO	64	0.698	0.625	0.562	0.339
1ATG	231	0.613	0.578	0.497	0.154
1BYI	224	0.543	0.491	0.552	0.133
1CCR	111	0.580	0.512	0.351	0.530
1E5K	188	0.746	0.732	0.859	0.620
1EW4	106	0.650	0.644	0.547	0.447
1IFR	113	0.697	0.689	0.637	0.330
1NKO	122	0.619	0.535	0.368	0.322
1NLS	238	0.669	0.530	0.523*	0.385
1O08	221	0.562	0.333	0.309	0.616
1PMY	123	0.671	0.654	0.685	0.702
1PZ4	114	0.828	0.781	0.843	0.844
1QTO	122	0.543	0.520	0.334	0.725
1RRO	112	0.435	0.372	0.529	0.546
1UKU	102	0.665	0.661	0.742	0.720
1V70	105	0.622	0.492	0.162	0.285
1WBE	204	0.591	0.577	0.549	0.574
1WHI	122	0.601	0.539	0.270	0.414
1WPA	107	0.634	0.577	0.417	0.380
2AGK	233	0.705	0.694	0.512	0.514
2C71	205	0.658	0.649	0.560	0.584
2CG7	90	0.551	0.539	0.379	0.308
2CWS	227	0.647	0.640	0.696	0.524
2HQK	213	0.824	0.809	0.365	0.743
2HYK	238	0.585	0.575	0.510	0.593
2I24	113	0.593	0.498	0.494	0.441
2IMF	203	0.652	0.625	0.514	0.401
2PPN	107	0.677	0.638	0.668	0.468
2R16	176	0.582	0.495	0.618*	0.411
2V9V	135	0.555	0.548	0.528	0.594
2VIM	104	0.413	0.393	0.212	0.221
2VPA	204	0.763	0.755	0.576	0.594
2VYO	210	0.675	0.648	0.729	0.739
3SEB	238	0.801	0.712	0.826	0.720
3VUB	101	0.625	0.610	0.607	0.365

Table 7: Correlation coefficients for B-factor prediction obtained by optimal FRI (opFRI), parameter free FRI (pfFRI) and Gaussian normal mode (GNM) for a set of 365 proteins. GNM scores reported here are the result of our tests with a processed set of PDB files as described in Section III.C

PDB ID	N	opFRI	pfFRI	GNM	PDB ID	N	opFRI	pfFRI	GNM
1ABA	87	0.727	0.698	0.613	1PEF	18	0.888	0.826	0.808
1AGN	1492	0.331	0.051	0.170	1PEN	16	0.516	0.465	0.270
1AHO	64	0.698	0.625	0.562	1PMY	123	0.671	0.654	0.685
1AIE	31	0.588	0.416	0.155	1PZ4	114	0.828	0.781	0.843
1AKG	16	0.373	0.350	0.185	1Q9B	43	0.746	0.726	0.656
1ATG	231	0.613	0.578	0.497	1QAU	112	0.678	0.672	0.620
1BGF	124	0.603	0.539	0.543	1QKI	3912	0.809	0.751	0.645
1BX7	51	0.726	0.623	0.706	1QTO	122	0.543	0.520	0.334
1BYI	224	0.543	0.491	0.552	1R29	122	0.650	0.631	0.556
1CCR	111	0.580	0.512	0.351	1R7J	90	0.789	0.621	0.368
1CYO	88	0.751	0.702	0.741	1RJU	36	0.517	0.447	0.431
1DF4	57	0.912	0.889	0.832	1RRO	112	0.435	0.372	0.529
1E5K	188	0.746	0.732	0.859	1SAU	114	0.742	0.671	0.596
1ES5	260	0.653	0.638	0.677	1TGR	104	0.720	0.711	0.714
1ETL	12	0.710	0.609	0.628	1TZV	141	0.837	0.820	0.841
1ETM	12	0.544	0.393	0.432	1U06	55	0.474	0.429	0.434
1ETN	12	0.089	0.023	-0.274	1U7I	267	0.778	0.762	0.691
1EW4	106	0.650	0.644	0.547	1U9C	221	0.600	0.577	0.522
1F8R	1932	0.878	0.859	0.738	1UHA	83	0.726	0.665	0.638
1FF4	65	0.718	0.613	0.674	1UKU	102	0.665	0.661	0.742
1FK5	93	0.590	0.568	0.485	1ULR	87	0.639	0.594	0.495
1GCO	1044	0.766	0.693	0.646	1UOY	64	0.713	0.653	0.671
1GK7	39	0.845	0.773	0.821	1USE	40	0.438	0.146	-0.142
1GVD	52	0.781	0.732	0.591	1USM	77	0.832	0.809	0.798
1GXU	88	0.748	0.634	0.421	1UTG	70	0.691	0.610	0.538
1H6V	2927	0.488	0.429	0.306	1V05	96	0.629	0.599	0.632
1HJE	13	0.811	0.686	0.616	1V70	105	0.622	0.492	0.162
1I71	83	0.549	0.516	0.549	1VRZ	21	0.792	0.695	0.677
1IDP	441	0.735	0.715	0.690	1W2L	97	0.691	0.564	0.397
1IFR	113	0.697	0.689	0.637	1WBE	204	0.591	0.577	0.549
1K8U	89	0.553	0.531	0.378	1WHI	122	0.601	0.539	0.270
1KMM	1499	0.749	0.744	0.558	1WLY	322	0.695	0.679	0.666
1KNG	144	0.547	0.536	0.512	1WPA	107	0.634	0.577	0.417
1KR4	110	0.635	0.612	0.466	1X3O	80	0.600	0.559	0.654
1KYC	15	0.796	0.763	0.754	1XY1	18	0.832	0.645	0.447
1LR7	73	0.679	0.657	0.620	1XY2	8	0.619	0.570	0.562
1MF7	194	0.687	0.681	0.700	1Y6X	87	0.596	0.524	0.366
1N7E	95	0.651	0.609	0.497	1YJO	6	0.375	0.333	0.434
1NKD	59	0.750	0.703	0.631	1YZM	46	0.842	0.834	0.901
1NKO	122	0.619	0.535	0.368	1Z21	96	0.662	0.638	0.433
1NLS	238	0.669	0.530	0.523	1ZCE	146	0.808	0.757	0.770
1NNX	93	0.795	0.789	0.631	1ZVA	75	0.756	0.579	0.690
1NOA	113	0.622	0.604	0.615	2A50	457	0.564	0.524	0.281
1NOT	13	0.746	0.622	0.523	2AGK	233	0.705	0.694	0.512
1O06	20	0.910	0.874	0.844	2AH1	939	0.684	0.593	0.521
1O08	221	0.562	0.333	0.309	2B0A	186	0.639	0.603	0.467
1OB4	16	0.776	0.763	0.750	2BCM	413	0.555	0.551	0.477
1OB7	16	0.737	0.545	0.652	2BF9	36	0.606	0.554	0.680
1OPD	85	0.555	0.409	0.398	2BRF	100	0.795	0.764	0.710
1P9I	29	0.754	0.742	0.625	2C71	205	0.658	0.649	0.560

Table 7 (cont.): Correlation coefficients for B-factor prediction obtained by optimal FRI (opFRI), parameter free FRI (pfFRI) and Gaussian normal mode (GNM) for a set of 365 proteins. GNM scores reported here are the result of our tests with a processed set of PDB files as described in Section III.C

PDB ID	N	opFRI	pfFRI	GNM	PDB ID	N	opFRI	pfFRI	GNM
2CE0	99	0.706	0.598	0.529	2OLX	4	0.917	0.888	0.885
2CG7	90	0.551	0.539	0.379	2PKT	93	0.162	0.003	-0.193
2COV	534	0.846	0.823	0.812	2PLT	99	0.508	0.484	0.509
2CWS	227	0.647	0.640	0.696	2PMR	76	0.693	0.682	0.619
2D5W	1214	0.689	0.682	0.681	2POF	440	0.682	0.651	0.589
2DKO	253	0.816	0.812	0.690	2PPN	107	0.677	0.638	0.668
2DPL	565	0.596	0.538	0.658	2PSF	608	0.526	0.500	0.565
2DSX	52	0.337	0.333	0.127	2PTH	193	0.822	0.784	0.767
2E10	439	0.798	0.796	0.692	2Q4N	153	0.711	0.667	0.740
2E3H	81	0.692	0.682	0.605	2Q52	412	0.756	0.748	0.621
2EAQ	89	0.753	0.690	0.695	2QJL	99	0.594	0.584	0.594
2EHP	248	0.804	0.804	0.773	2R16	176	0.582	0.495	0.618
2EHS	75	0.720	0.713	0.747	2R6Q	138	0.603	0.540	0.529
2ERW	53	0.461	0.253	0.199	2RB8	93	0.727	0.614	0.517
2ETX	389	0.580	0.556	0.632	2RE2	238	0.652	0.613	0.673
2FB6	116	0.791	0.786	0.740	2RFR	154	0.693	0.671	0.753
2FG1	157	0.620	0.617	0.584	2V9V	135	0.555	0.548	0.528
2FN9	560	0.607	0.595	0.611	2VE8	515	0.744	0.643	0.616
2FQ3	85	0.719	0.692	0.348	2VH7	94	0.775	0.726	0.596
2G69	99	0.622	0.590	0.436	2VIM	104	0.413	0.393	0.212
2G7O	68	0.785	0.784	0.660	2VPA	204	0.763	0.755	0.576
2G7S	190	0.670	0.644	0.649	2VQ4	106	0.680	0.679	0.555
2GKG	122	0.688	0.646	0.711	2VY8	149	0.770	0.724	0.533
2GOM	121	0.586	0.584	0.491	2VYO	210	0.675	0.648	0.729
2GXG	140	0.847	0.780	0.520	2W1V	548	0.680	0.680	0.571
2GZQ	191	0.505	0.382	0.369	2W2A	350	0.706	0.638	0.589
2HQK	213	0.824	0.809	0.365	2W6A	117	0.823	0.748	0.647
2HYK	238	0.585	0.575	0.510	2WJ5	96	0.484	0.440	0.357
2I24	113	0.593	0.498	0.494	2WUJ	100	0.739	0.598	0.598
2I49	398	0.714	0.683	0.601	2WW7	150	0.499	0.471	0.356
2IBL	108	0.629	0.625	0.352	2WWE	111	0.692	0.582	0.628
2IGD	61	0.585	0.481	0.386	2X1Q	240	0.534	0.478	0.443
2IMF	203	0.652	0.625	0.514	2X25	168	0.632	0.598	0.403
2IP6	87	0.654	0.578	0.572	2X3M	166	0.744	0.717	0.655
2IVY	88	0.544	0.483	0.271	2X5Y	171	0.718	0.705	0.694
2J32	244	0.863	0.848	0.855	2X9Z	262	0.583	0.578	0.574
2J9W	200	0.716	0.705	0.662	2XHF	310	0.606	0.591	0.569
2JKU	35	0.805	0.695	0.656	2Y0T	101	0.778	0.774	0.798
2JLI	100	0.779	0.613	0.622	2Y72	170	0.780	0.754	0.766
2JLJ	115	0.741	0.720	0.527	2Y7L	319	0.928	0.797	0.747
2MCM	113	0.789	0.713	0.639	2Y9F	149	0.771	0.762	0.664
2NLS	36	0.605	0.559	0.530	2YLB	400	0.807	0.807	0.675
2NR7	194	0.803	0.785	0.727	2YNY	315	0.813	0.804	0.706
2NUH	104	0.835	0.691	0.771	2ZCM	357	0.458	0.422	0.420
2O6X	306	0.814	0.799	0.651	2ZU1	360	0.689	0.672	0.653
2OA2	132	0.571	0.456	0.458	3A0M	148	0.807	0.712	0.392
2OCT	192	0.567	0.550	0.540	3A7L	128	0.713	0.663	0.756
2OHW	256	0.614	0.539	0.475	3AMC	614	0.675	0.669	0.581
2OKT	342	0.433	0.411	0.336	3AUB	116	0.614	0.608	0.637
2OL9	6	0.909	0.904	0.689	3B5O	230	0.644	0.629	0.601

Table 7 (cont.): Correlation coefficients for B-factor prediction obtained by optimal FRI (opFRI), parameter free FRI (pfFRI) and Gaussian normal mode (GNM) for a set of 365 proteins. GNM scores reported here are the result of our tests with a processed set of PDB files as described in Section III.C

PDB ID	N	opFRI	pfFRI	GNM	PDB ID	N	opFRI	pfFRI	GNM
3BA1	312	0.661	0.624	0.621	3MD4	12	0.860	0.781	0.914
3BED	261	0.845	0.820	0.684	3MD5	12	0.649	0.413	-0.218
3BQX	139	0.634	0.481	0.297	3MEA	166	0.669	0.669	0.600
3BZQ	99	0.532	0.516	0.466	3MGN	348	0.205	0.119	0.193
3BZZ	100	0.485	0.450	0.600	3MRE	383	0.661	0.641	0.567
3DRF	547	0.559	0.549	0.488	3N11	325	0.614	0.583	0.517
3DWV	325	0.707	0.661	0.547	3NE0	208	0.706	0.645	0.659
3E5T	228	0.502	0.489	0.296	3NGG	94	0.696	0.689	0.719
3E7R	40	0.706	0.687	0.642	3NPV	495	0.702	0.653	0.677
3EUR	140	0.431	0.427	0.577	3NVG	6	0.721	0.617	0.597
3F2Z	149	0.824	0.792	0.740	3NZL	73	0.627	0.583	0.506
3F7E	254	0.812	0.803	0.811	3O0P	194	0.727	0.706	0.734
3FCN	158	0.640	0.606	0.632	3O5P	128	0.734	0.698	0.630
3FE7	91	0.583	0.533	0.276	3OBQ	150	0.649	0.645	0.655
3FKE	250	0.525	0.476	0.435	3OQY	234	0.698	0.686	0.637
3FMY	66	0.701	0.655	0.556	3P6J	125	0.774	0.767	0.810
3FOD	48	0.532	0.440	-0.126	3PD7	188	0.770	0.723	0.589
3FSO	221	0.831	0.817	0.793	3PES	165	0.697	0.642	0.683
3FTD	240	0.722	0.713	0.634	3PID	387	0.537	0.531	0.642
3FVA	6	0.835	0.825	0.789	3PIW	154	0.758	0.744	0.717
3G1S	418	0.771	0.700	0.630	3PKV	221	0.625	0.597	0.568
3GBW	161	0.820	0.747	0.510	3PSM	94	0.876	0.790	0.745
3GHJ	116	0.732	0.511	0.196	3PTL	289	0.543	0.541	0.468
3HFO	197	0.691	0.670	0.518	3PVE	347	0.718	0.667	0.568
3HHP	1234	0.720	0.716	0.683	3PZ9	357	0.709	0.709	0.678
3HNY	156	0.793	0.723	0.758	3PZZ	12	0.945	0.922	0.950
3HP4	183	0.534	0.500	0.573	3Q2X	6	0.922	0.904	0.866
3HWU	144	0.754	0.748	0.841	3Q6L	131	0.622	0.577	0.605
3HYD	7	0.966	0.950	0.867	3QDS	284	0.780	0.745	0.568
3HZ8	192	0.617	0.502	0.475	3QPA	197	0.587	0.442	0.503
3I2V	124	0.486	0.441	0.301	3R6D	221	0.688	0.669	0.495
3I2Z	138	0.613	0.599	0.317	3R87	132	0.452	0.419	0.286
3I4O	135	0.735	0.714	0.738	3RQ9	162	0.510	0.403	0.242
3I7M	134	0.667	0.635	0.695	3RY0	128	0.616	0.606	0.470
3IHS	169	0.586	0.565	0.409	3RZY	139	0.800	0.784	0.849
3IVV	149	0.817	0.797	0.693	3S0A	119	0.562	0.524	0.526
3K6Y	227	0.586	0.535	0.301	3SD2	86	0.523	0.421	0.237
3KBE	140	0.705	0.704	0.611	3SEB	238	0.801	0.712	0.826
3KGK	190	0.784	0.775	0.680	3SED	124	0.709	0.658	0.712
3KZD	85	0.647	0.611	0.475	3SO6	150	0.675	0.666	0.630
3L41	220	0.718	0.716	0.669	3SR3	637	0.619	0.611	0.624
3LAA	169	0.827	0.647	0.659	3SUK	248	0.644	0.633	0.567
3LAX	106	0.734	0.730	0.584	3SZH	697	0.817	0.815	0.697
3LG3	833	0.658	0.614	0.589	3T0H	208	0.808	0.775	0.694
3LJI	272	0.612	0.608	0.551	3T3K	122	0.796	0.748	0.735
3M3P	249	0.584	0.554	0.338	3T47	141	0.592	0.527	0.447
3M8J	178	0.730	0.728	0.628	3TDN	357	0.458	0.419	0.240
3M9J	210	0.639	0.574	0.296	3TOW	152	0.578	0.556	0.571
3M9Q	176	0.591	0.510	0.471	3TUA	210	0.665	0.658	0.588
3MAB	173	0.664	0.591	0.451	3TYS	75	0.853	0.800	0.791

Table 7 (cont.): Correlation coefficients for B-factor prediction obtained by optimal FRI (opFRI), parameter free FRI (pfFRI) and Gaussian normal mode (GNM) for a set of 365 proteins. GNM scores reported here are the result of our tests with a processed set of PDB files as described in Section III.C

PDB ID	N	opFRI	pfFRI	GNM	PDB ID	N	opFRI	pfFRI	GNM
3U6G	248	0.635	0.632	0.526	4DT4	160	0.776	0.738	0.716
3U97	77	0.753	0.736	0.712	4EK3	287	0.680	0.680	0.674
3UCI	72	0.589	0.526	0.495	4ERY	318	0.740	0.701	0.688
3UR8	637	0.666	0.652	0.597	4ES1	95	0.648	0.625	0.551
3US6	148	0.698	0.586	0.553	4EUG	225	0.570	0.529	0.405
3V1A	48	0.531	0.487	0.583	4F01	448	0.633	0.372	0.688
3V75	285	0.604	0.596	0.491	4F3J	143	0.617	0.598	0.551
3VN0	193	0.840	0.837	0.812	4FR9	141	0.671	0.655	0.501
3VOR	182	0.602	0.557	0.484	4G14	15	0.467	0.323	0.356
3VUB	101	0.625	0.610	0.607	4G2E	151	0.760	0.755	0.758
3VVV	108	0.833	0.741	0.753	4G5X	550	0.786	0.754	0.743
3VZ9	163	0.785	0.749	0.695	4G6C	658	0.591	0.590	0.528
3W4Q	773	0.737	0.725	0.649	4G7X	194	0.688	0.587	0.624
3ZBD	213	0.651	0.516	0.632	4GA2	144	0.528	0.485	0.406
3ZIT	152	0.430	0.404	0.392	4GMQ	92	0.678	0.628	0.550
3ZRX	221	0.590	0.562	0.391	4GS3	90	0.544	0.522	0.547
3ZSL	138	0.691	0.687	0.526	4H4J	236	0.810	0.806	0.689
3ZZP	74	0.524	0.460	0.448	4H89	168	0.682	0.588	0.596
3ZZY	226	0.746	0.709	0.728	4HDE	168	0.745	0.728	0.615
4A02	166	0.618	0.516	0.303	4HJP	281	0.703	0.649	0.510
4ACJ	167	0.748	0.746	0.759	4HWM	117	0.638	0.622	0.499
4AE7	186	0.724	0.717	0.717	4IL7	85	0.446	0.404	0.316
4AM1	345	0.674	0.619	0.460	4J11	357	0.620	0.562	0.401
4ANN	176	0.551	0.536	0.470	4J5O	220	0.793	0.757	0.777
4AVR	188	0.680	0.605	0.650	4J5Q	146	0.742	0.742	0.689
4AXY	54	0.700	0.623	0.720	4J78	305	0.658	0.648	0.608
4B6G	558	0.765	0.756	0.669	4JG2	185	0.746	0.736	0.543
4B9G	292	0.844	0.816	0.763	4JVU	207	0.723	0.697	0.553
4DD5	387	0.615	0.596	0.351	4JYP	534	0.688	0.682	0.538
4DKN	423	0.781	0.761	0.539	4KEF	133	0.580	0.530	0.324
4DND	95	0.763	0.750	0.582	5CYT	103	0.441	0.421	0.331
4DPZ	109	0.730	0.726	0.651	6RXN	45	0.614	0.574	0.594
4DQ7	328	0.690	0.683	0.376					

Table 8: CPU execution times (in seconds) from efficiency comparison between FRI, fFRI and GNM

PDB ID	N	FRI	fFRI	GNM
3P6J	125	*	*	0.141
3R87	132	*	*	0.156
3KBE	140	*	*	0.187
1TZV	141	*	*	0.203
2VY8	149	*	*	0.219
3ZIT	152	*	*	0.234
2FG1	157	*	*	0.265
2X3M	166	*	*	0.312
3LAA	169	*	*	0.327
3M8J	178	*	*	0.375
2GZQ	191	*	*	0.468
4G7X	194	*	*	0.499
2J9W	200	*	*	0.546
3TUA	210	*	*	0.655
1U9C	221	*	*	0.733
3ZRX	221	*	*	0.718
3K6Y	227	*	*	0.765
3OQY	234	*	*	0.873
2J32	244	*	*	0.967
3M3P	249	*	*	1.029
1U7I	267	*	*	1.263
4B9G	292	*	*	1.669
4ERY	318	*	*	2.122
3MGN	348	*	*	2.902
2ZU1	360	*	*	3.136
2Q52	412	*	*	4.696
4F01	448	*	*	6.178
3DRF	547	0.062	*	11.154
3UR8	637	0.07	*	17.409
2AH1	939	0.156	*	61.012
1GCO	1044	0.187	*	75.801
1AGN	1492	0.343	*	298.632
1F8R	1932	0.655	*	654.127
1H6V	2927	1.545	*	2085.842
1QKI	3912	2.699	*	6365.668
3KGV	4064	2.949	*	6194.518
1K32	6138	6.755	*	*
1JZ0	8168	11.87	*	*
4BGR	8949	14.056	0.889	*
1VSZ	12012	25.413	1.248	*
GroEL	14700	*	1.467	*
B Gal	16336	*	1.716	*
1VRI	18540	*	1.934	*
HIV	313236	*	29.344	*